4

RESULTS AND DISCUSSION

Pseudomonas aeruginosa is a virulent Gram-negative bacterium that can infect people with impaired immune systems (Thi *et al.*, 2020). The risk of mortality exhibited by *Pseudomonas aeruginosa* infections has increased due to the organism's inherent resistance to conventional antibiotics and its adaptability to them (Pang *et al.*, 2019). The formation of biofilms, the first step in the pathogenesis of *Pseudomonas aeruginosa*, is triggered by an integrated signaling pathway referred to as quorum sensing (QS). The QS in *Pseudomonas aeruginosa* has three key systems: LasR, RhlR, and PqsR. The transcriptional receptors of these QS systems sense their corresponding autoinducers (AIs) to regulate the genes involved in formation of biofilm and other physiological activities (Mukherjee and Bassler, 2019).

Though each of the three QS systems is distinct, they are connected hierarchically, with the *las* system influencing the others and its associated receptor protein LasR being recognized as the essential protein involved in regulating a variety of virulence-related traits (Asfahl and Schuster, 2018). Researchers have also shown that the QS circuit governs a wide range of physiological processes and specifically focusing on the *las* system may be an effective strategy for controlling *Pseudomonas aeruginosa* pathogenesis (Sarkar *et al.*, 2018).

Computer Aided Drug Discovery (CADD) is becoming more and more popular in drug discovery for identifying compounds from the hit-to-lead process (Ahamed *et al.*, 2019). *In silico* computational approaches can deduce biological and chemical details about the ligands and protein (Lokhande *et al.*, 2019). Different computational tools, such as the pharmacological assessment, quantitative structure-activity relationship (QSAR), and techniques such as molecular docking and simulation, have completely transformed the platform of drug discovery (Ahamed *et al.*, 2019). Numerous methods have been tried so far to find a good lead like molecule with antiquorum sensing and antibiofilm capabilities for treating infections linked to *Pseudomonas aeruginosa*. But the literature on experimental and modeling investigations has stated that the rate of bacterial resistance to the discovered quorum sensing inhibitors (QSIs) is increasing steadily (García-Contreras *et al.*, 2013).

In the present study, molecular docking-based virtual screening was performed to find an effective inhibitor for LasR. The compounds with notably greater docking scores were chosen and assessed for their pharmacologic characteristics. The molecular dynamics simulation study was employed to demonstrate the stability in interactions of the selected compounds with the target protein. Finally, the selected compounds were purchased, and the cytotoxicity was assessed in human peripheral blood lymphocyte cells. The compounds were then validated through *in vitro* assays for their antibiofilm and antiquorum sensing properties. Furthermore, the gene expression pattern of the quorum sensing regulatory genes on treatment with selected inhibitors was analyzed by qRT-PCR. Their ability to inhibit LasR at the transcriptional level was confirmed by an *in vitro* β-galactosidase reporter gene assay. The salient findings of the present research work are discussed as follows.

4.1. Phase I: Virtual screening of inhibitors against LasR of *Pseudomonas aeruginosa* and molecular dynamics simulation study

4.1.1. Analysis of the structure of target protein LasR

The three-dimensional (3D) crystal structure of the LasR of *Pseudomonas aeruginosa* with **PDB ID: 3IX4** was obtained from the Protein Data Bank (PDB). Examination of the retrieved structure demonstrated that the protein is a cocrystallized structure with a bound molecule TP-1 (triphenyl mimic of the natural inducer) which is an agonist and with the resolution of 1.8 Å. TP-1 is a signal mimic of the native autoinducer of LasR and possesses enhanced specificity towards LasR (Müh *et al.*, 2006). The ligand binding domain of the cocrystallized structure (3IX4) was found to be made up of five β-sheet strands antiparallelly flanked on either side by six strands of α-helices (Figure 11).

In general, the autoinducer of LasR, N-(3-oxo-dodecanoyl)-L-homoserine lactone (OdDHL) interacts with LasR and activates the QS pathway when it is present at a quorate concentration. Observation of the active pocket of LasR inferred that the polar head group of the native ligand established hydrogen bond interactions with the residues Tyr56, Trp60, Asp73 and Ser129. In contrast, the autoinducer's non-polar tail group interacted with hydrophobic residues Leu125, Val76, Ile52, Leu40, and Leu36 in the binding site of LasR (Figure 12).

Figure 11
Cocrystallized structure of the LasR-TP-1 complex

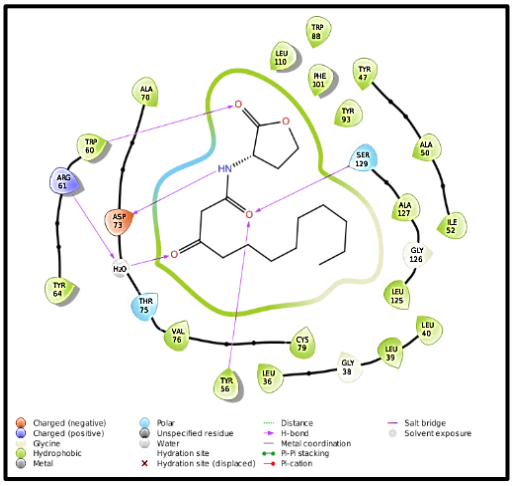

Figure 12
2D Ligand interaction diagram of native autoinducer (OdDHL) with LasR

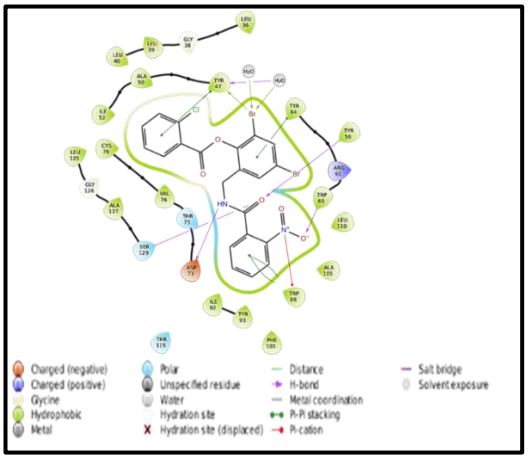

Figure 13
2D Ligand interaction diagram of TP-1 (triphenyl mimic of autoinducer) with LasR

The non-bonded interaction protect the ligand binding site of LasR from bulk solvents and traps the hydrophobic residues close to the binding site. As a result, LasR is then stabilized in its active homodimer form. As a result of polar and non-polar interactions, the stabilized LasR homodimer-ligand complex dimerizes, with the central interface consisting of two loop and two helix regions. The dimerized LasR structure binds to specific promoters and induce expression of genes related to QS (Zou and Nair, 2009).

Observing the ligand binding site of the PDB (3IX4) revealed that TP-1 formed five direct and one water-mediated intermolecular hydrogen bond interactions with Ser129, Thr75, Asp73, Arg61, Trp60, and Tyr56. Particularly, the polar head group of TP-1 was engaged in hydrogen bond interactions similar to that of autoinducer involving residues Tyr56, Trp60, Asp73, and Ser129 (Figure 13). It is already well established that the LuxR homologs share a high degree of conservation for the residues Tyr56, Trp60, Asp73, and Ser129.

4.1.2. *In silico* identification of quorum sensing inhibitors against LasR by high throughput virtual screening

4.1.2.1. Structure based virtual screening

Initially, 3,034,496 compounds from the Schrödinger small molecule database were virtually screened to find compounds that interacted with LasR. Of these, 1,942,018 compounds were obtained as hits in the high throughput virtual screening (HTVS) mode. Standard precision (SP) mode of docking was then performed on the top 10% of the compounds obtained from HTVS, which ordered molecules based on docking scores. The top 10% of the compounds from SP docking were then subjected to flexible extra precision (XP) docking mode, which involved 19,420 compounds. One thousand nine hundred and forty two compounds were finally obtained at the end of XP docking. The overall workflow of the HTVS process is provided in Figure 14.

To determine a threshold docking score, we performed docking of several known inhibitors of LasR with 3IX4 (Plate 1) and the results are provided in Table 8. Binding free energy was used as the scoring function in virtual screening process. The outcomes revealed that Gscore varied between -6.0 to -11.0 kcal/mol (Table 8). The correlation (R^2) between glide energy and pIC_{50} of the known active compounds was found to be 0.5078. Hence, a Gscore of < -11.0 kcal/mol was established as the criteria for filtering in the virtual screening

process to screen potential inhibitors against LasR. Based on this criteria, 12 compounds with a docking score of < -11.0 kcal/mol were chosen as the top hits from the list of XP docked compounds. The docking scores and the hydrogen bond contacts of the top hits are shown in Table 9.

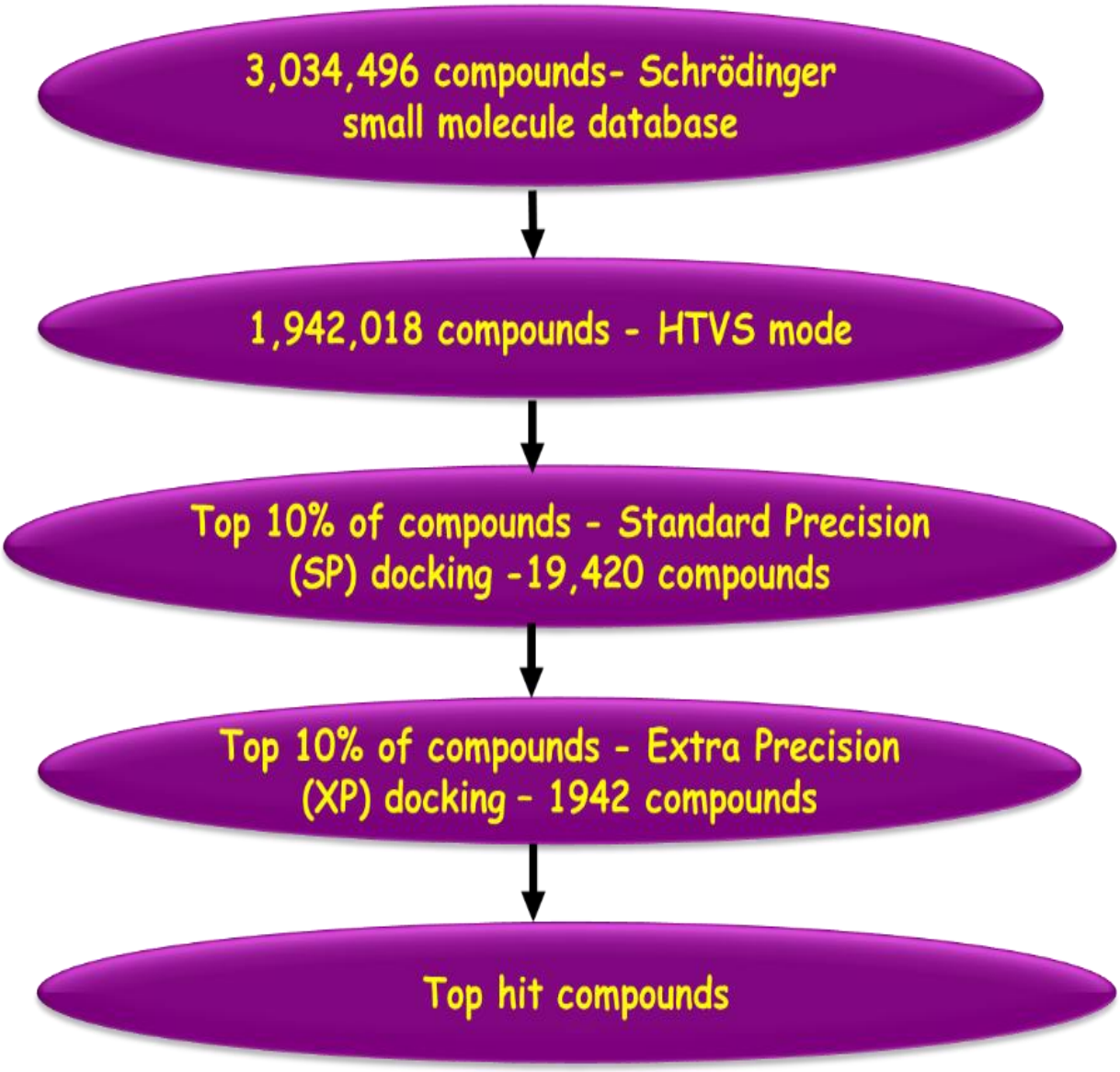

Figure 14

Workflow of the HTVS process for selection of potent LasR inhibitors

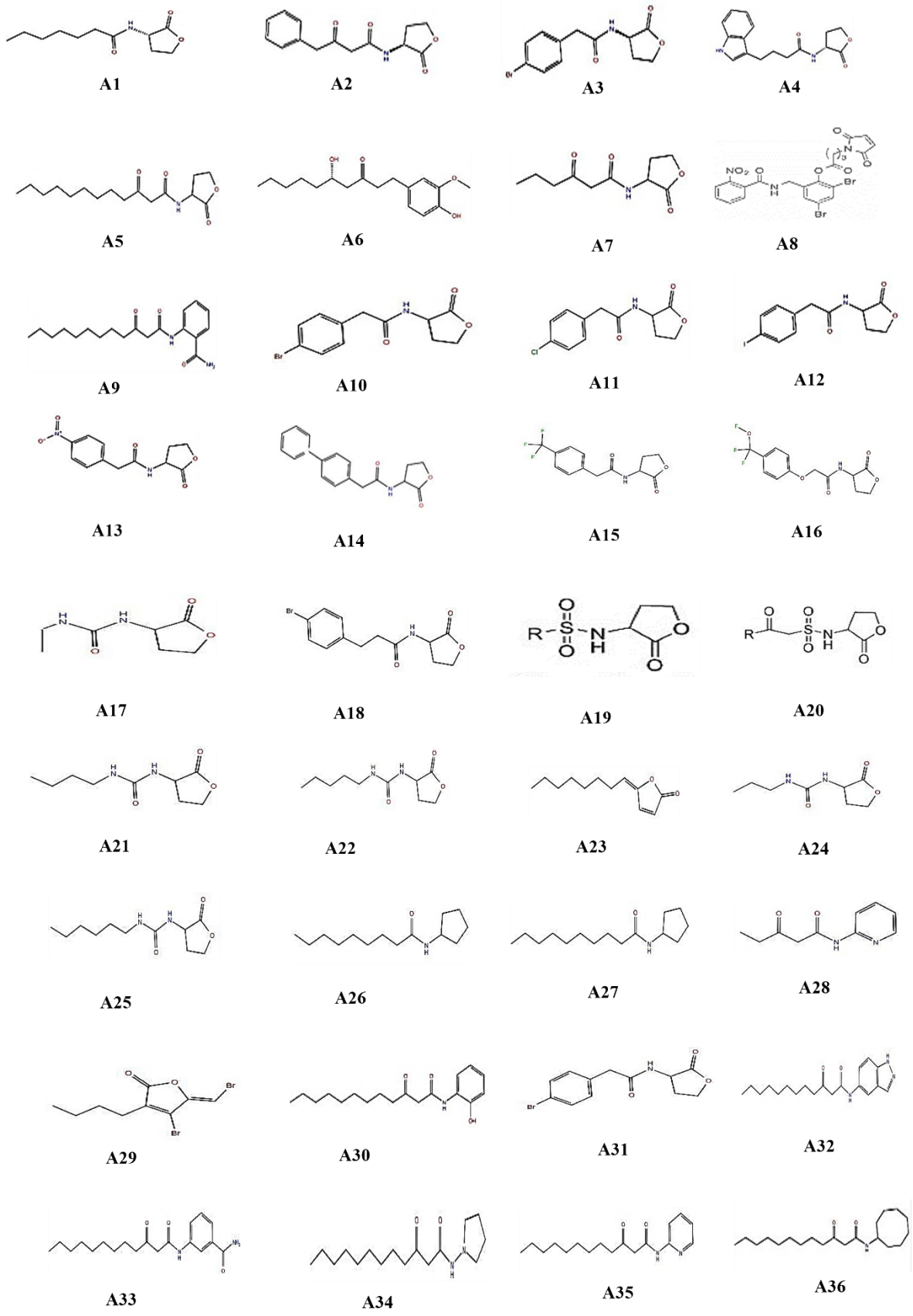

Plate 1
Structures of the known antagonists collected from literatures

Table 8
Molecular docking study of known antagonists with LasR (3IX4)

Antagonist	pIC50 value (µM)	Docking score (kcal/mol)	H-bond interaction residues	References
A1	5.9	**-11.158**	Tyr47, Tyr56, Trp60, Asp73, Ser129	Geske *et al.*, 2008
A2	5.0	**-10.183**	Tyr56, Asp73, Tyr93, Ser129	
A3	5.6	**-9.481**	Tyr56, Trp60, Asp73, Ser129	
A4	7.0	**-9.457**	Tyr56, Ser129	
A5	5.3	**-9.456**	Tyr47, Arg61, Tyr93	O'Brien *et al.*, 2015
A6	6.5	**-9.451**	Tyr56, Asp73, Ser129	Choi *et al.*, 2017
A7	4.0	**-9.189**	Tyr56, Asp73, Ser129	O'Reilly *et al.*, 2018
A8	6.0	**-9.071**	Tyr56, Asp73, Ser129	
A9	5.7	**-8.644**	Arg61, Trp60, Tyr56, Asp73, Ser129	Smith *et al.*, 2003
A10	4.0	**-8.623**	Asp73, Ser129	Ni *et al.*, 2008
A11	4.0	**-8.514**	Thr75, Ser129	
A12	4.0	**-8.431**	Arg61	
A13	5.6	**-8.396**	Thyr56, Ser129	
A14	5.2	**-8.396**	Arg61, Tyr47, Tyr93	
A15	5.6	**-8.289**	Tyr56, Asp73, Ser129	
A16	4.0	**-7.969**	Tyr56, Asp73, Ser129	
A17	5.6	**-7.949**	Val76, Ser129	

Contd..

Contd..

Antagonist	pIC50 value (µM)	Docking score (kcal/mol)	H-bond interaction residues	References
A18	5.3	**-7.934**	Val56, Asp73, Ser129	
A19	4.3	**-7.875**	Asp73, Tyr56, Ser129	Ni *et al.*, 2008
A20	4.3	**-7.714**	Trp60, Tyr56, Asp73, Ser129	
A21	4.3	**-7.659**	Tyr56, Asp73, Ser129	
A22	5.8	**-7.567**	Tyr56, Ser129	
A23	5.4	**-7.598**	Arg61	
A24	5.3	**-7.45**	Tyr56, Ser129	
A25	6.04	**-7.45**	Arg61, Tyr47, Tyr93	
A26	6.0	**-7.448**	Tyr56, Asp73, Ser129	
A27	5.9	**-7.421**	Tyr56, Asp73, Ser129	
A28	6.2	**-7.417**	Val76, Ser129	
A29	5.7	**-7.368**	Val56, Asp73, Ser129	
A30	6.2	**-7.347**	Asp73, Tyr56, Ser129	Smith *et al.*, 2003
A31	5.3	**-7.346**	Asp73, Arg61, Tyr56, Ser129	
A32	8.0	**-7.191**	Tyr56	
A33	9.0	**-7.136**	Tyr56, Trp60, Asp73, Ser129	
A34	6.4	**-7.074**	Tyr56, Trp60, Asp73	
A35	6.08	**-7.029**	Thr75, Ser129	
A36	4.2	**-6.918**	Trp60, Tyr56, Asp 73, Ser129	

The top three compounds (Table 9) that exhibited the highest XP docking scores, namely CACPD2011a-0001928786 - (3-[2-(3,4-dimethoxyphenyl) -2- (1H- indol-3-yl)ethyl]-1-(2-fluorophenyl)urea), CACPD2011a-0001927437 - (3-(4-fluorophenyl)-2-[(3-methylquinoxalin-2-yl) methylsulfanyl] quinazolin-4-one), CACPD2011a-0000896051 - (2-({4- [4- (2-methoxyphenyl) piperazin-1-yl] pyrimidin - 2 - yl} sulfanyl) - N - (2,4,6 trimethylphenyl) acetamide) were chosen and was given designations as C1, C2, and C3, respectively.

Among the three compounds, C1 possesses chiral centers, however the other isomers included in the first screening list were absent in the final deck of compounds obtained from the XP docking. Hence, this finding strongly indicated the significant stereospecificity of C1 for LasR compared to the other two compounds. The 2D structures of the compounds selected for the present study are shown in Figure 15.

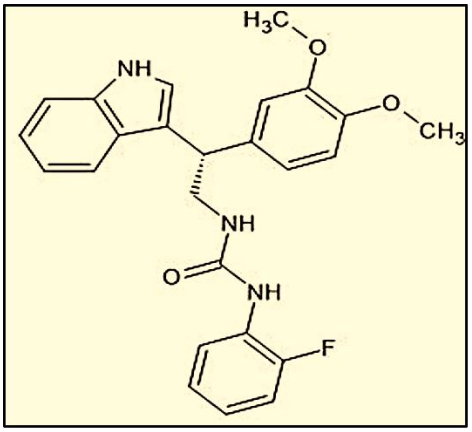

CACPD2011a-0001928786 (C1)

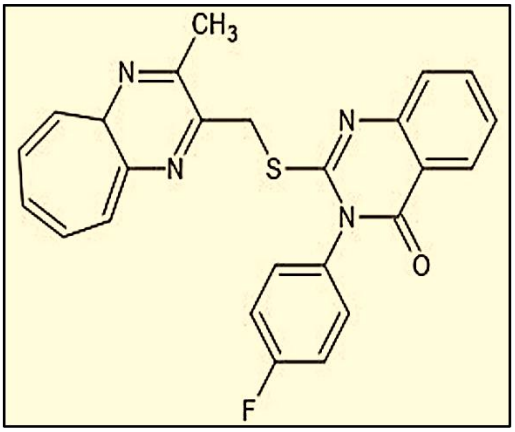

CACPD2011a-0001927437 (C2)

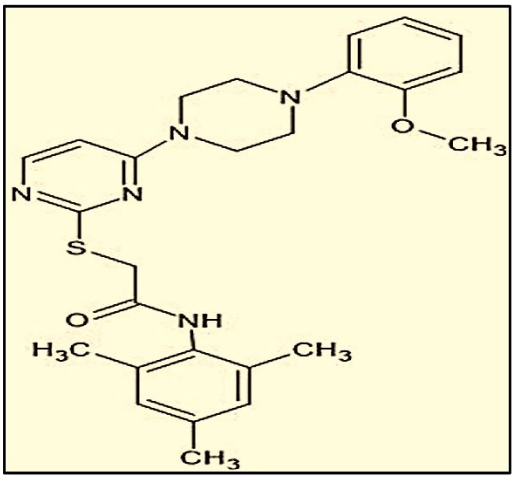

CACPD2011a-0000896051 (C3)

Figure 15
2D structures of the selected compounds

Table 9
Docking scores and hydrogen bond interactions of the top 12 hit compounds obtained from XP docking

Compounds	XP docking score (kcal/mol)	No. of H-bonds	Residues involved in H-bond interaction
Native ligand (Autoinducer-OdDHL)	-7.5	4	Try56, Trp60, Asp73, Ser129
TP-1 (Triphenyl mimic of autoinducer)	-12.8	4	Try56, Trp60, Asp73, Ser129
CACPD2011a-0001928786	**-13.0**	**3**	**Try56, Asp73, Ser129**
CACPD2011a-0001927437	**-12.2**	**3**	**Try56, Asp73, Ser129**
CACPD2011a-0000896051	**-11.7**	**0**	**-**
CACPD2011a-0001779781	-11.7	2	Try56, Ser129
CACPD2011a-0001734913	-11.6	0	-
CACPD2011a-0002367758	-11.4	3	Try56, Trp60, Ser129
CACPD2011a-0002145356	-11.3	1	Try56
CACPD2011a-0001893654	-11.2	0	-
CACPD2011a-0002017222	-11.1	2	Try56, Ser129
CACPD2011a-0002215130	-11.1	3	Try56, Asp73, Thr115
CACPD2011a-0002142621	-11.0	1	Ser129
CACPD2011a-0000661063	-11.0	3	Try56, Asp73, Leu110

4.1.2.2. Protein-ligand interaction

The pattern of interactions between the selected inhibitors and the target protein is demonstrated by the protein-ligand interaction profile of the docked complexes. An extensive examination of the complexes revealed that hydrogen bonds, hydrophobic interactions, π-π interactions, polar and charged positive contacts, play a vital role in the binding of selected

compounds into the active pocket of LasR. The 2D ligand interaction pattern of the selected compounds with target LasR is depicted in Figure 16.

Figure 16a shows that C1 interacted with the residues Tyr56, Ser129, and Asp73 via hydrogen bonds. The residues Tyr47, Ala50, Leu39, Ile52, Ala127, Leu40, Leu125, Tyr64, Cys79, Trp60, Val76, Leu36, Leu110, Tyr56, Ala105, Phe101, Trp88, and Tyr93 made hydrophobic interactions with C1. C1 demonstrated π-π interactions with Trp88, Tyr64, Phe 101, and Trp60. In the instance of C2 (Figure 16b), the residues Tyr56, Ser129, and Asp73 were involved in hydrogen bond networking. Amino acid residues Phe101 and Tyr47 were engaged in π-π interaction. Hydrophobic interactions were facilitated by amino acid residues Tyr93, Ala105, Phe101, Trp60, Tyr56, Leu36, Ala50, Tyr64, Leu39, Ile52, Leu40, Val76, Tyr47, Ala127, Cys 79, Leu125, and Leu110.

In contrast, compound C3 (Figure 16c) made no hydrogen bond interactions but demonstrated hydrophobic interactions with the residues Ala127, Ile52, Tyr47, Tyr64, Val76, Trp60, Cys79, Tyr56, Leu125, Leu110, Leu40, Ala105, Ala50, Phe101, Leu39, Tyr93, Leu36, and Trp88. Tyr47, Trp88, Phe101, and Tyr64 amino acids were found to be engaged in π-π contacts. Arg61 was the only amino acid residue involved in positive charged interactions with all three selected compounds. Conversely, C1 and C2 displayed polar contacts with Thr75 and Ser129, while C3 generated polar contacts via amino acids Ser129, Thr75, and Thr119.

Among the non-bonding interactions, the hydrogen bonding pattern of ligands with the amino acid residues of protein provide directionality and specificity, which is essential for the steady and accurate fitting of ligands into the binding pocket of the target protein (Qiu *et al.*, 2018). Therefore, we have examined the hydrogen bonding pattern of the chosen compounds with the target LasR to evaluate their antagonistic potential further.

The activators OdDHL and TP-1 formed four hydrogen bond contacts with binding site residues of LasR, namely Tyr56, Trp60, Asp73, and Ser129. On the contrary, the hydrogen bond interaction patterns of the top 12 ranked hits differed utterly from those of the native inducers OdDHL and TP-1 (Table 9). Additionally, the molecular docking analysis of the known antagonists (Table 8) also revealed that only six molecules out of 36 formed hydrogen bond interactions with all the four active site residues of LasR, namely Tyr56, Trp60, Asp73, and Ser129.

In concordance with our results, Sadiq *et al.* (2020) witnessed six molecules that were found to be potent inhibitors against LasR in *Pseudomonas aeruginosa* and did not possess hydrogen bond interactions with all four of the binding site residues Tyr56, Trp60, Asp73, and Ser129. Nain *et al.* (2020) also stated that the inhibitors of LasR form non-bonding interactions that were not similar to those of the native inducers. Sharma *et al.* (2019b) noted that hydrocinnamic acid obtained from *Enterobacter xianfangensis* was found to be effective in inhibiting LasR of *Pseudomonas aeruginosa*, and it also demonstrated hydrogen bonding connections involving only Tyr56, Asp73, and Ser129 residues and π-π contact with Phe101.

Kalia *et al.* (2017) retrieved seven putative inhibitors of LasR from a preliminary database in PyRX which also did not exhibit hydrogen bond interactions with all of the active site amino acid residues of LasR. Bottomley *et al.* (2007) reported that a potent LasR agonist should generate hydrogen bonds with all four of the amino acid residues and be able to fill the active site pocket of LasR. The LasR inhibitors did not exhibit hydrogen bond interactions with all four crucial residues Tyr56, Trp60, Asp73, and Ser129 in the active pocket of protein may attribute to its QS inhibitory activity.

Zou and Nair (2009), by analysis of X-ray crystallographic structure of LasR bound with autoinducer (OdDHL) and TP-1 (Triphenyl mimic of autoinducer), stated that Trp60 holds a crucial role in the function of LasR. In the present study, C1 and C2 formed hydrogen bonds with only three (Tyr56, Asp73, Ser129) of the four crucial amino acid residues, while C3 completely lacked hydrogen bond interaction (Figure 16). It is also noted that C1 and C2 did not establish hydrogen bond with Trp60.

O'Reilly *et al.* (2018) stated that the ligands which failed to generate a hydrogen bond contact with Trp60 in LasR acted as strong antagonists. Tan *et al.* (2013) discovered three QSIs namely 2-amino-3-(3-fluorophenyl) propanoic acid, indole-3-carboxylic acid, and 2-amino-3-hydroxy-3-phenyl propanoic acid and reported that the identified QSIs did not interact with Trp60 via hydrogen bonds. A LasR-patulin complex model described by Bottomley *et al.* (2007) revealed that patulin which imitates the lactone of AHLs and could activate LasR formed a conventional hydrogen bond with Trp60. In line with the above literatures, docking study also revealed that all three selected compounds did not establish hydrogen bond with Trp60 and may act as potent inhibitors of LasR.

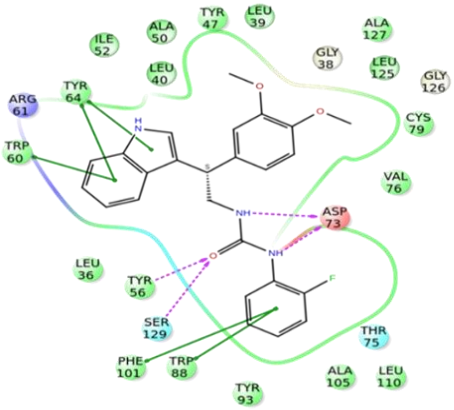

a) CACPD2011a-0001928786 (C1)

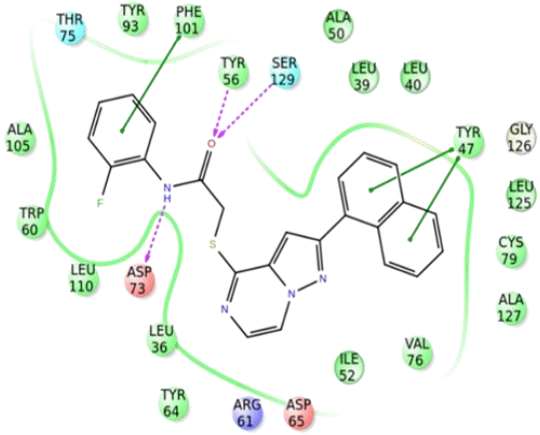

b) CACPD2011a-0001927437 (C2)

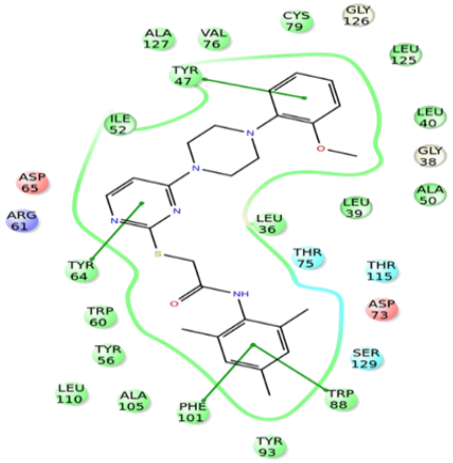

c) CACPD2011a-0000896051 (C3)

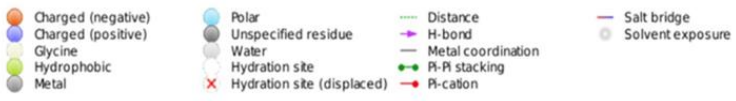

Figure 16
2D ligand interaction of the selected compounds with LasR (3IX4)

4.1.3. Calculation of binding free energy of the docked complexes

4.1.3.1. Prime MM-GBSA

The MM-GBSA method was employed as a post-docking analysis tool as it offers a better correlation between the experimental and predicted binding affinities (Borkotoky *et al.*, 2016). Therefore the post-docking assessment of the docked complexes was performed by calculating binding free energy (ΔG_{Bind}) of the complexes using the prime MM-GBSA method in Schrödinger software. The method focused on different energy calculations, such as Coulomb energy, lipophilic energy, *van der Waals* energy, solvation energy, and strain energy of the ligands, to demonstrate the affinity of the ligands to bind to the active pocket of the target. The results of the binding free energy calculation of the complexes are provided in Table 10.

The results revealed that the values of the dissociated binding free energies of the selected compounds ranged between -92.2 and -112.2 kcal/mol. The MM-GBSA free energy calculation showed that the native inducer and TP-1 exhibited binding free energies of -93.7 and -147.4 kcal/mol, respectively. Among the selected compounds, C2 had the highest binding free energy (-112.2 kcal/mol), while C3 had the lowest (-92.2 kcal/mol). The Coulomb energies of the complexes (ΔG_{Coul}) portrayed that C1 had the most incredible Coulomb energy (-59.2 kcal/mol) than the other complexes.

The polar solvation energy calculated based on the implicit solvation model VSGB 2.0, implied that C1 had the maximum solvation energy of 65.4 kcal/mol followed by C3 (35.6 kcal/mol) and C2 (28.2 kcal/mol). The post-docking analysis revealed that C1 possesses the highest Coulomb and solvation energy. C2 exhibited the highest binding free energy. C3 demonstrated a higher binding affinity in terms of lipophilic energy, *van der Waals* energy, and strain energy of ligands whose corresponding values were -68.6, -65.7, and 37.3 kcal/mol.

Casalvieri *et al.* (2020) suggested that greater negative value indicates stronger binding as the MM-GBSA binding energies are approximations of free energies of binding. Nazar *et al.* (2020) stated that the active site interacting residues, which exhibit binding free energies of <-1 kcal/mol determined by the MM-GBSA method, has a significant contribution towards the stability of the protein-ligand complexes. Hence, these results

inferred that the compounds chosen in the present study exhibited good binding free energy scores and are more likely to be favorable for stable binding with the target LasR.

Table 10
Post docking analysis of the selected compounds by prime MM-GBSA

Compounds	ΔG_{Bind} (kcal/mol)	ΔG_{Coul} (kcal/mol)	ΔG_{Lipo} (kcal/mol)	ΔG_{vdW} (kcal/mol)	ΔG_{SolvGB} (kcal/mol)	SE_{Lig} (kcal/mol)
Native ligand	-93.7	-16.7	-44.2	-49.3	16.0	13.5
TP-1	-147.4	-20.8	-63.2	-78.0	21.7	3.3
C1	-103.6	-59.2	-49.9	-61.0	65.4	14.9
C2	-112.2	-19.9	-54.3	-61.7	28.2	16.3
C3	-92.2	-3.0	-68.6	-65.7	35.6	37.3

ΔG_{Bind} - MM-GBSA free binding energy; ΔG_{Coul} - Coulomb energy of the complex; ΔG_{Lipo} - lipophilic energy of the complex; ΔG_{vdW} - *van der Waals* energy of the complex; ΔG_{SolvGB} - solvation energy of the complex; SE_{Lig} - strain energy of the ligands

4.1.4. ADMET and drug-likeness prediction

One of the biggest shortcomings observed throughout the clinical studies is the poor pharmacokinetic profile exhibited by the lead molecules. Therefore, it would be advantageous if these problems were dealt with at an earlier stage. Using *in silico* technology to anticipate potential pharmacokinetic characteristics and the drug-likeness properties of hits would be more beneficial for identifying the best lead-like molecules (Pal *et al.*, 2019). The QikProp v5.8 module of the Schrödinger software was employed to investigate the pharmacokinetic profile and drug-like features of the selected LasR inhibitors. The results obtained are given in Table 11.

A drug's effectiveness and safety are determined by its bioavailability which relies mainly on drug absorption and the liver's first-pass metabolism (Opo *et al.*, 2021). QikProp considers several factors for determining the bioavailability of a drug, namely Jorgensen's Rule of Three (RO3), conformation-independent predicted aqueous solubility (CIQPlogS), predicted human oral absorption (pHOA), and qualitative human oral absorption. QPlogS, #metab, and QPPCaco are the three components of RO3 used to monitor the intestinal absorption of orally administered drugs. In the case of RO3, all selected compounds showed only one violation. The aqueous solubility and the number of expected metabolic processes

are predicted by QPlogS and #metab (Shahbazi *et al.,* 2016). The predicted #metab of the chosen compounds was within the recommended range.

On the contrary, except for C1, the QPlogS of C2 and C3 falls outside the reference range. Caco-2 cell permeability (QPPCaco) serves as the gut-blood barrier model, and MDCK cells permeability (QPPMDCK) mimics the blood-brain barrier (BBB) (Arora *et al.,* 2019). It is revealed that QPPCaco and QPPMDCK were within the range for all three compounds. The selected compounds were observed to have CIQPlogS value outside the acceptable range of existing drugs. However, all the selected compounds had the highest percentage of human oral absorption (pHOA). The capacity of the selected inhibitors to bind to human serum albumin (HSA) was predicted using the QikProp parameter $QPlogK_{hsa}$. The results portrayed that the capacity of the selected compounds to bind HSA was within the range of permissible values, indicating that they would attach to HSA with a reduced affinity and eventually make them more accessible for binding to the target.

The $QPlogH_{ERG}$ value is a crucial measure for identifying cardiac and neurotoxicity. Failure in heart functions may occur if a drug interacts with the HERG K^+ channel. The findings revealed that the predicted log IC_{50} values for blockage of HERG K^+ channels of all three selected compounds were less than -5, which fell within the concerned range. The $QPlogK_p$ values of all the selected compounds were relatively low, indicating their low permeation ability to skin. The BBB permeability of the compounds was assessed by the predicted central nervous system (CNS) activity and the predicted brain/blood partition coefficient (QPlogBB) values. The CNS activity and QPlogBB values of all three compounds were within the reference range.

Correlation between the hydrophobicity and permeability values is vital to determine the best drug candidate (Arora *et al.,* 2019). For a lead molecule to be effective, it should be able to cross various barriers and possess better permeability performance. For complete absorption and distribution of the drug, there should be a balance between drug's hydrophobic and hydrophilic property. The $QPlogP_{O/W}$ is a vital descriptor used to measure the compound's lipophilicity. Lipophilicity is related to the permeability of the compounds across the biological membranes. The ideal value of $QPlogP_{O/W}$ should be intermediate and not too high or too low (Kumar *et al.,* 2011). Here, C1 and C2 have an intermediate $QPlogP_{O/W}$, whereas C3 had a slightly higher $QPlogP_{O/W}$ value.

Table 11
ADMET and drug-likeness properties of the selected compounds

ADMET/drug-likeness properties	Compounds			Reference range (in 95% drugs)
	C1	C2	C3	
Predicted polarizability in cubic angstroms (QPPolrz)	46.4	49.8	53.4	13.0 to 70.0
Predicted hexane/gas partition coefficient ($QPlogP_{C16}$)	14.4	13.9	15.1	4.0 to 18.0
Predicted octanol/gas partition coefficient ($QPlogP_{oct}$)	21.9	20.1	23.2	8.0 to 35.0
Predicted water/gas partition coefficient ($QPlogP_{W}$)	12.0	9.9	10.9	4.0 to 45.0
Predicted octanol/water partition coefficient ($QPlogP_{O/W}$)	5.2	5.4	6.0	-2.0 to 6.5
Predicted aqueous solubility (QPlogS)	-6.3	-7.2	-7.7	-6.5 to 0.5
Conformation-independent predicted aqueous solubility (CIQPlogS)	-6.9	-6.9	-7.4	-6.5 to 0.5
Predicted IC_{50} value for blockage of HERG K+ channels ($QPlogH_{ERG}$)	-5.2	-7.0	-6.3	Concern below -5
Predicted apparent Caco-2 cell permeability in nm/s (QPPCaco)	1551.8	2414.1	3749.9	<25=poor; >500=great
No. of primary metabolites (#metab)	4	3	6	1.0 to 8.0
Predicted brain/blood partition coefficient (QPlogBB)	-0.5	-0.2	-0.1	-3.0 to 1.2
Predicted apparent MDCK cell permeability in nm/s (QPPMDCK)	1566.7	2610.7	3581.6	<25=poor; >500=great
Predicted skin permeability (QPlogKp)	-0.8	-1.0	-0.9	-8.0 to -1.0
Prediction of binding to human serum albumin ($QPlogK_{hsa}$)	0.7	0.8	1.1	-1.5 to 1.5
Predicted human oral absorption (pHOA)	100	100	100	<25% is poor
Predicted central nervous system activity (CNS)	-1	0	0	-2 to +2
Number of violations of the 95% range (#stars)	0	1	1	-
Number of violations of Lipinski's rule of five (V_{R05})	1	1	1	Maximum is 4
Number of violations of Jorgensen's rule of three (V_{R03})	1	1	1	Maximum is 3

Finally, a drug candidate for active oral medication should not violate more than one rule of Lipinski's "Rule of Five" criteria (Lipinski *et al.,* 2001). The rule evaluates the drug-like characteristics of any lead drug candidate, including molecular weight, hydrogen bond acceptors and donors, and logP (Jana *et al.,* 2018). The result indicates that the selected compounds showed only one violation of Lipinski's Rule of five; hence they can be regarded as drug-like.

In QikProp, the #stars parameter describes the number of descriptors not within the acceptable range of values determined for 95% of the known drugs. In this context, C1 exhibited zero violations while C2 and C3 displayed one violation. The ADMET and drug-likeness property analysis revealed that the selected inhibitors could serve as possible leads as they adhere to all the pharmacokinetic and drug-likeness requirements.

4.1.5. Molecular dynamics simulation

Molecular dynamics (MD) is a simulation approach used to track and assess the actual motions of atoms and molecules. It offers comprehensive details on the rigidity, fluctuations, flexibility and conformational alterations of biological molecules and their complexes throughout the simulation. Due to the convergence of the sequence of amino acids at various time steps during the process of simulation, the conformational flexibility of a receptor changes due to its interaction with the ligand (Manzoor *et al.,* 2021; Lokhande *et al.,* 2019; Rajendran *et al.,* 2018).

Molecular dynamics simulation was carried out for 100 ns using Desmond v5.6 package of Schrödinger software. This study was undertaken to witness the binding stability of protein-ligand complexes, and to understand the binding mode and the type of interactions holding the selected compounds within the LasR's ligand binding site. The parameters of MD simulation, namely root mean square deviation (RMSD), root mean square fluctuation (RMSF), interaction map of protein-ligand complexes, the radius of gyration (R_g) and intramolecular hydrogen bonds, were analyzed to explore the binding mode of LasR in its bound state with tested compounds.

4.1.5.1. Root mean square deviation (RMSD) analysis

RMSD is determined by lining up the structures created during the MD simulation process in the trajectory with that of the initial frame (Kumar *et al.,* 2019). The RMSD of

Cα, sidechain, backbone and heavy atoms of protein and ligand fit protein are calculated during the entire time frames of the simulation process (100 ns). The results of MD trajectories calculated in terms of RMSD for LasR in the apo form and in the presence of ligands are shown in Figure 17 (a-d).

The RMSD of the protein in presence of C1 remained constant at about 1.25 Å over a 100 ns simulation (Figure 17a). On the other hand, the RMSD of LasR-C2 complex was found to fluctuate up to 60 ns before becoming remarkably stable around 1.2 Å (Figure 17b). Figure 17c shows that the RMSD of the LasR-C3 complex was at 1.0 Å till 18 ns, after that, it jumped to 4.2 Å. But, beyond 20 ns, it was stable at 3.0 Å throughout the simulation period. There were minor deviations in RMSD observed in all three protein complexes, but they were insignificant.

Figure 17 (a-c) also clearly shown that the ligand RMSD was much smaller than the RMSD of protein. The LasR's apo form was stabilized and equilibrated for a period of 100 ns. The apo form of LasR was stabilized at 2.4 Å throughout the simulation process (Figure 17d). The difference in RMSD value of ligand bound complex and apo form was less than 3.0 Å.

Jana *et al.* (2018) stated that RMSD of ligand-acetylcholinesterase complex converged between 1.5-2.5 Å during a 50 ns simulation period. Opo *et al.* (2021) reported that RMSD fluctuations between 1-3 Å are entirely acceptable. And values considerably higher than this suggest that the protein has undergone a significant conformational shift and the system is unstable. Nain *et al.* (2020) identified two LasR inhibitors against *Pseudomonas aeruginosa* namely ZINC19765885 and ZINC72387263 and that the average RMSD values obtained during a 65 ns simulation process were around 1.65 Å and 1.67 Å, respectively.

Ramanathan *et al.* (2019) suggested that difference in RMSD value of protein-ligand complex and its apo form over 3.0 Å may indicate that the overall topology of the protein was changed and led to an unstable complex. In line with the above literatures, the RMSD analysis of the present study suggested that the selected compounds did not diffuse away from the active site of LasR over the entire simulation time.

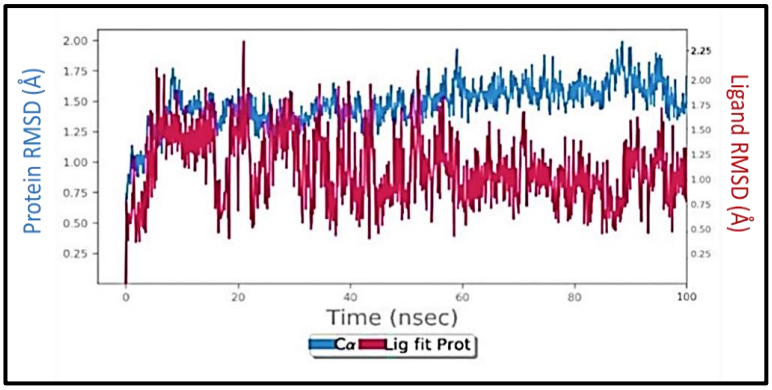

a) LasR-C1 complex

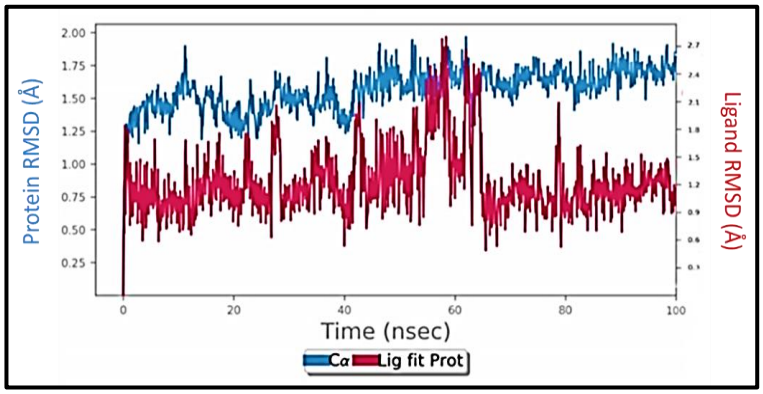

b) LasR-C2 complex

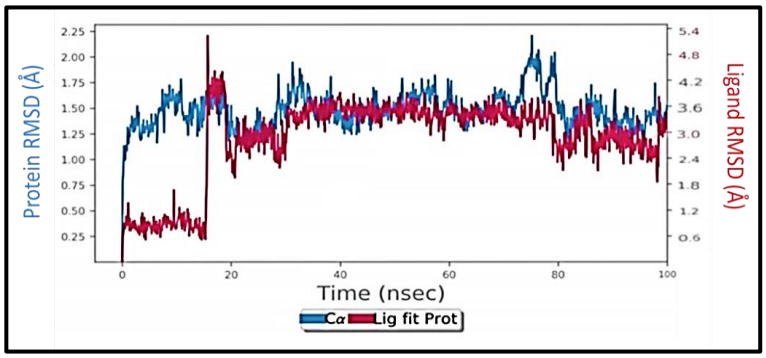

c) LasR-C3 complex

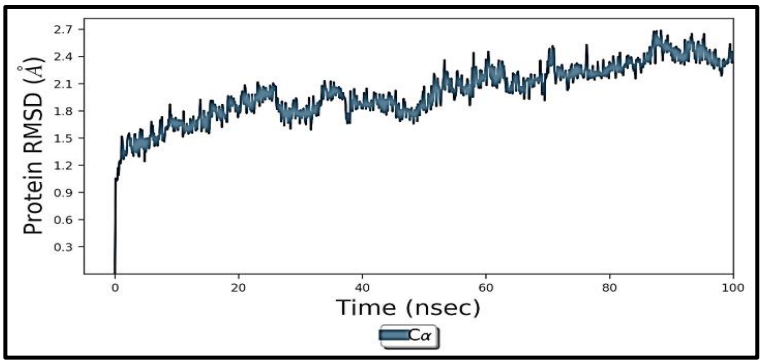

d) Apo form of LasR

Figure 17

RMSD of LasR in complex with selected compounds and its apo form

4.1.5.2. Root mean square fluctuation analysis

The role of every amino acid residue in maintaining the stability of the protein-ligand complex was examined using root mean square fluctuation (RMSF) analysis. RMSF describes local variations in the Cα backbone of the protein chain and the peaks indicating the regions of the protein that fluctuated the greatest during the simulation. RMSF of all amino acid residues is used to assess the average variation in fluctuations of the docked complexes during the simulation process (Nazar *et al.*, 2020).

RMSF measurements are collected from the trajectory run by calculating the least square fitting to a beginning structure which is used as a reference frame. Generally, the N- and C- terminals of a protein chain fluctuate to a greater extent than any other protein region. This type of divergence in amino acid residues may be due to the flexible loop in that area and the absence of interactions with the appropriate ligands (Pal *et al.*, 2019).The RMSF analysis of the docked complexes and apo form of LasR for a period of 100 ns is depicted in Figure 18 (a-d).

The RMSF value of the LasR-C1 complex was 1.5 Å whereas on the binding of C2, the RMSF value was observed to be 1.7 Å. In the case of C3, the RMSF value 1.3 Å (Figure 18 (a-c)). The RMSF analysis reveals that C1 is having less fluctuation compared to C2 and C3. Figure 18d shows that apo protein exhibited a maximum RMSF value of 2.0 Å and it was maintained during the entire simulation period of 100 ns.

Jana *et al.* (2018) stated that RMSF values below 4.0 Å suggest that the ligand-protein complex is more stable and side chains underwent less conformational changes during the simulation. Hendi *et al.* (2022) reported that higher RMSF values indicates greater amino acid residues fluctuation. The RMSF analysis of the present study revealed that upon binding of selected compounds to LasR, there were only minor fluctuations in the protein residues untill the end of simulation process. These results prove that the selected compounds did not significantly affect the structural conformation and were in stable association with LasR.

Secondary structure of the protein

The changes in the secondary structure elements (SSE) of the protein namely alpha helices and beta strands on binding of selected compounds and in apo form during the simulation are depicted as timeline plots in Figure 19-22.

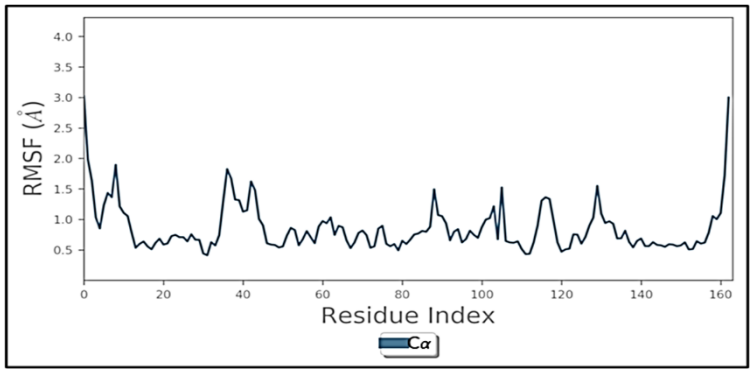

a) LasR-C1 complex

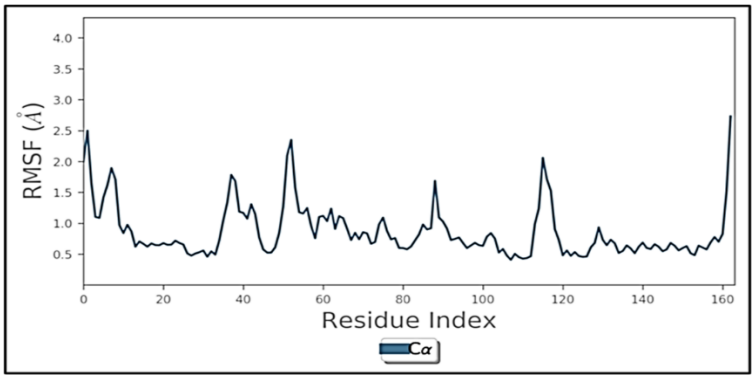

b) LasR-C2 complex

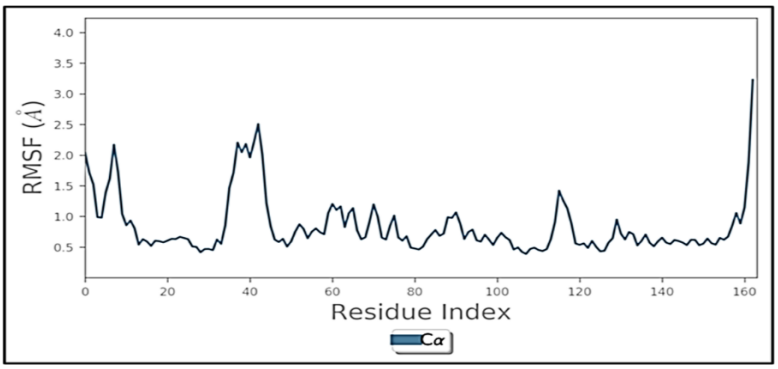

c) LasR-C3 complex

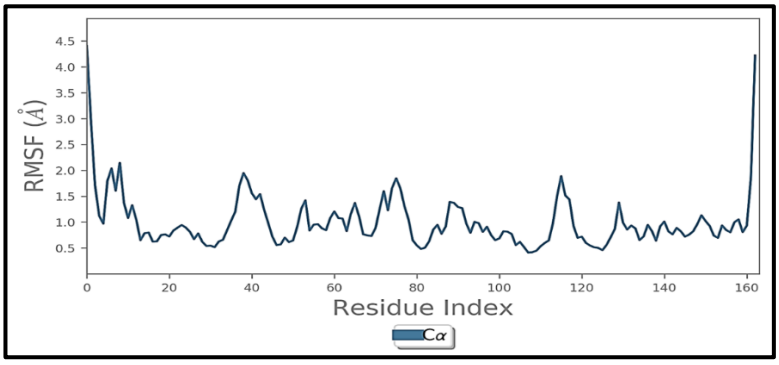

d) Apo form of LasR

Figure 18

RMSF of LasR in complex with selected compounds and its apo form

From Figure 19, it is inferred that when C1 binds to LasR, it exhibits 57.67% of secondary structure elements, of which 42.83% were alpha helices, and 14.84% were beta strands. When C2 binds to LasR (Figure 20), the percentage of secondary structure elements in LasR was 58.11%, where alpha-helical structures contributed to about 43.03% and beta strands made up to 15.08%.

The LasR on the binding of C3 (Figure 21) revealed a total secondary structure element of 56.87%. Among these elements, 41.20% were made of alpha helices, and 15.67% were found to be beta strands. When LasR is in its apo state (Figure 22), it exhibited approximately 50.75% of secondary structure elements, of which around 36.47% were alpha helices and about 14.28% were beta strands throughout the protein structure during the simulation of 100 ns.

Ligand RMSF

Ligand RMSF plots reveal information about the interactions of various fragments of compounds with the target and their entropic role in the binding process. Hence in the present study, the variations in the atom position of the selected compounds on binding to LasR were observed by ligand RMSF. The internal atomic fluctuations within the selected compounds during the 100 ns simulation are provided as ligand RMSF plots in Figure 23 (a-c).

The C1 (Figure 23a) and C2 (Figure 23b) on binding to LasR initially showed a very slighter hike in the RMSF value due to minor fluctuation but eventually decreased and maintained constant at 1.0 Å till the end of the simulation. Whereas the C3 (Figure 23c), showed an RMSF value of 2.0-2.5 Å for 50% of simulation time but after that drastically decreased and reached an RMSF of 1.0 Å to maintain a stable bound state with LasR.

When atoms are exposed to solvent molecules, more fluctuations are noticed in lead compounds and lower or lack of changes are observed when it is bound to the protein binding site (Manoharan *et al.*, 2021). Thus, the ligand RMSF plot proves that the compounds were held by the strong interaction of amino acid residues in the binding pocket of LasR throughout the simulation.

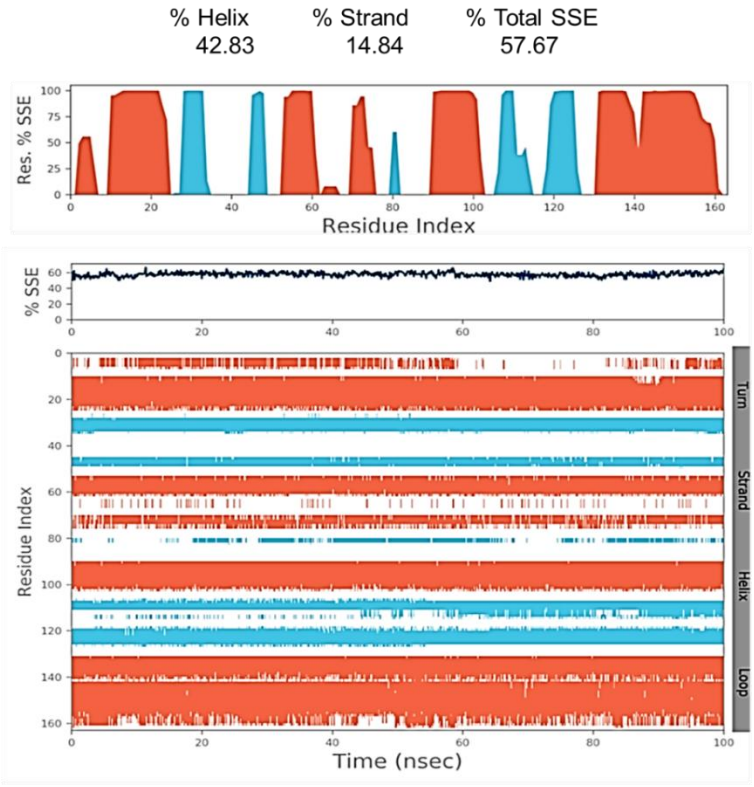

Figure 19
Changes in the secondary structure elements (SSE) of LasR on binding of C1

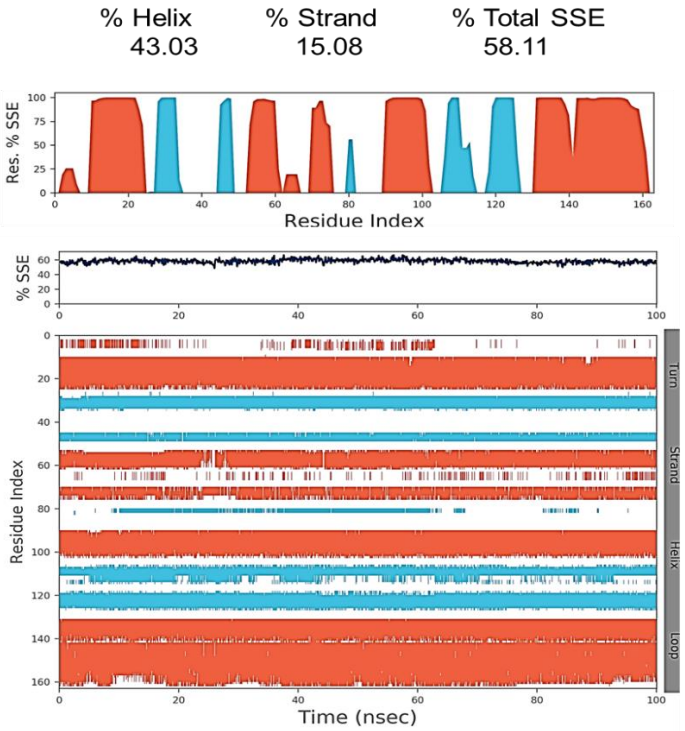

Figure 20
Changes in the secondary structure elements (SSE) of LasR on binding of C2

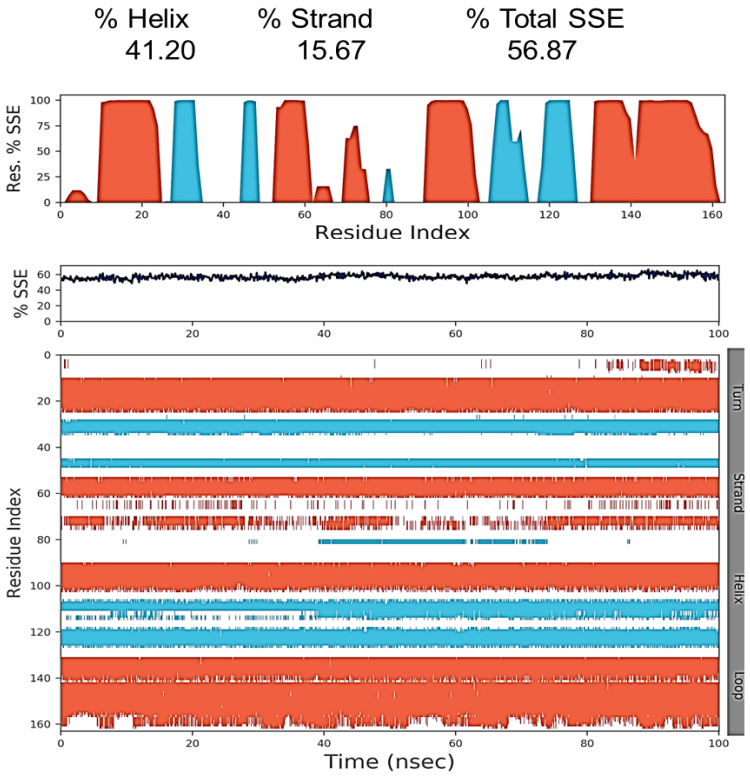

Figure 21
Changes in the secondary structure elements (SSE) of LasR on binding of C3

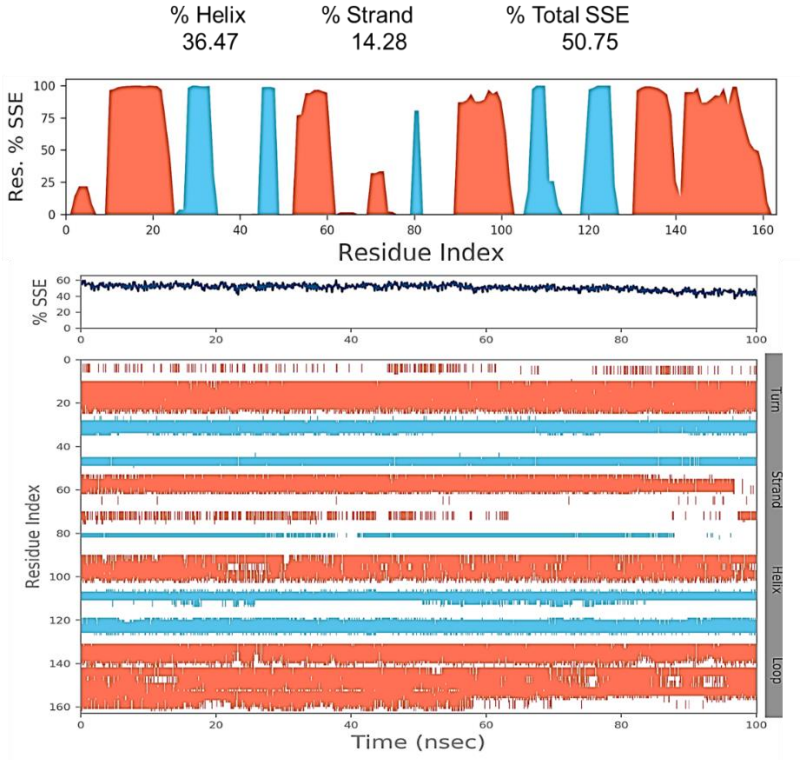

Figure 22
Changes in the secondary structure elements (SSE) of LasR (apo form)

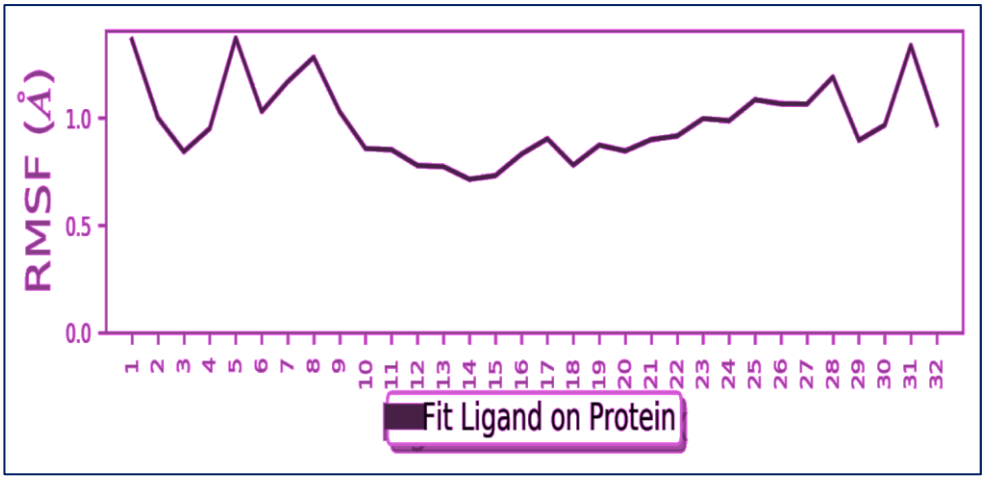

a) LasR-C1 complex

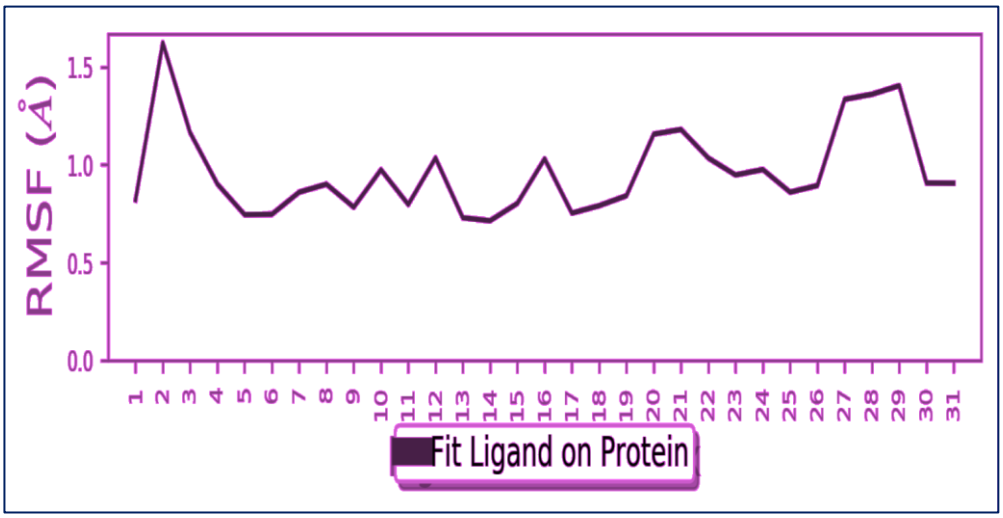

b) LasR-C2 complex

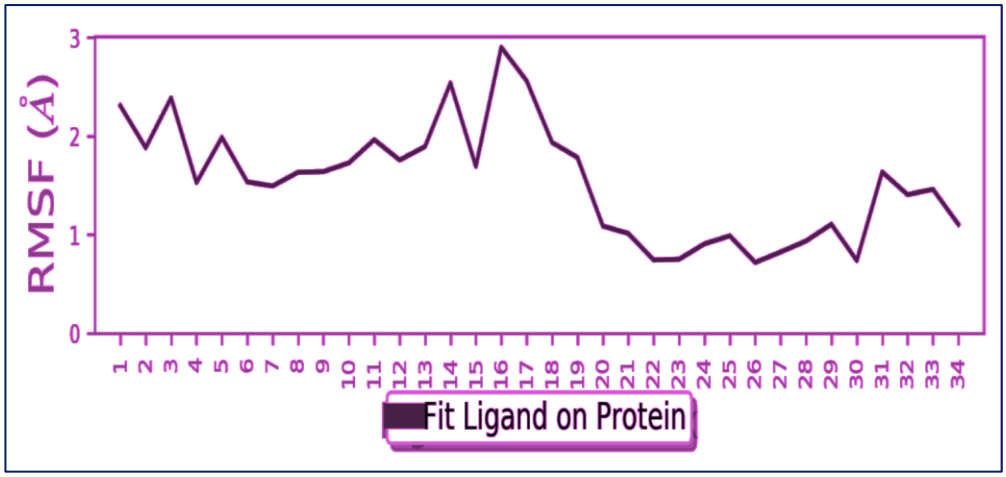

c) LasR-C3 complex

Figure 23

Ligand RMSF plots depicting the fluctuations of C1, C2, and C3 on binding to LasR

4.1.5.3. Protein-ligand interaction analysis

Analysis of the several non-bonded interactions between the ligand and protein would pave way to assess the stability of the ligand binding position (Arba *et al.,* 2018). The interaction between the protein and the ligand, which takes place through water bridges, hydrogen bonds, ionic bonds, and hydrophobic bonds is important in the development of an effective drug candidate (Opo *et al.,* 2021). The interactions between LasR and the selected compounds examined during the simulation are shown in Figure 24.

Histogram plots of the LasR complex revealed that compounds C1, C2, and C3 bind with LasR through non-bonded interactions in active pocket amino acid residues. From Figure 24a, it is observed that C1 forms hydrogen bond contacts with residues Gly38, Ser129, Leu39, Ala127, Phe51, Asp73, Tyr56, Tyr64, and Arg61. The interaction with residues Tyr56, Asp73, and Ser129 is retained from the docked pose (Figure 16a). The residue Asp73 interacted for more than 100% of the simulation time due to its multiple contacts with C1 (Figure 24a).

C1 form hydrophobic interaction with the residues Leu36, Ala127, Leu40, Leu110, Tyr47, Ala105, Ala50, Phe101, Ile52, Trp88, Tyr56, Cys79, Trp60,Val76, and Tyr64 (Figure 24a). It also reveals that C1 forms water bridges with residues Thr115, Arg61, Ser129, and Thr75. The residues Thr115 and Arg61 have interaction fractions of 0.5 and 0.8, suggesting that the water bridge formation of these residues with C1 is maintained over 30% of the simulation time (Plate 2a). C1 established interaction with Phe101, Trp88, and Tyr64. In addition to these residues, π-π interaction with Trp60 is also seen in the docked pose (Figure 16a).

Figure 24b avow that C2 forms hydrogen bond contacts with amino acids Ser129 and Tyr56. Among these two residues, C2 maintains hydrogen bond contact with Tyr56 for greater than 40% of the entire simulation time. The ligand interaction diagram of the docked pose of C2 affirms three hydrogen bond contacts with residues Tyr56, Asp73, and Ser129 (Figure 16b). In MD simulation, the hydrogen bond interactions with Tyr56 and Ser129 are retained. The residues Leu36, Ala127, Leu40, Leu125, Tyr64, Tyr56, Val76, Tyr47, Leu110, Ile52, Trp60, Ala105, Phe102, Phe101, Tyr93, and Trp88 were involved in hydrophobic contacts. Asp73 and Tyr93 form a water bridge with C2 for above 80% of the total simulation time (Plate 2b). In docked pose, C2 formed π-π interaction with amino acids Phe101 and Tyr47 (Figure 16b). In contrast, the ligand-protein interaction diagram of the simulated

complex revealed that C2 is engaged in π-π interaction with Tyr64 for greater than 60% of the total simulation period (Plate 2b).

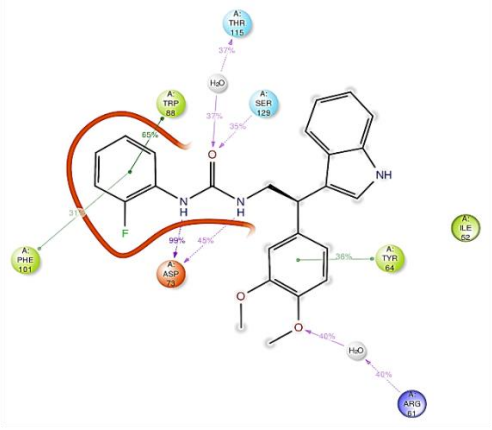

a) LasR-C1 contacts occurring more than 30% of simulation time

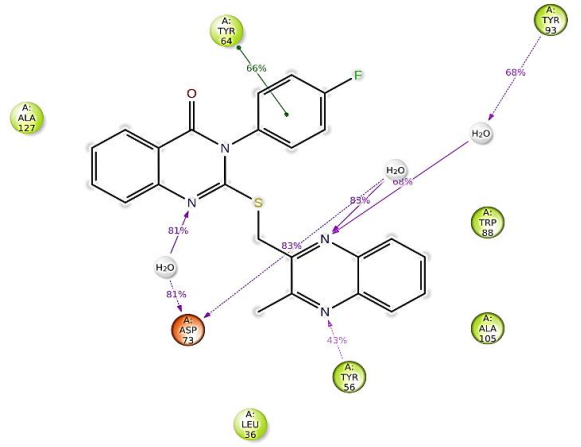

b) LasR-C2 contacts occurring more than 30% of simulation time

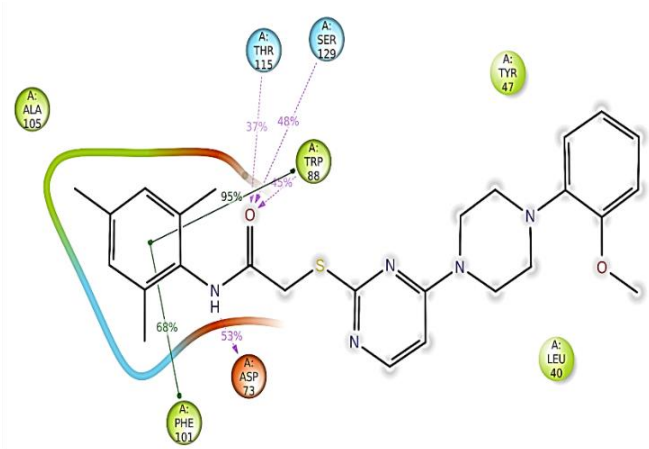

c) LasR-C3 contacts occurring more than 30% of simulation time

Plate 2

Analysis of molecular interaction of selected compounds with LasR

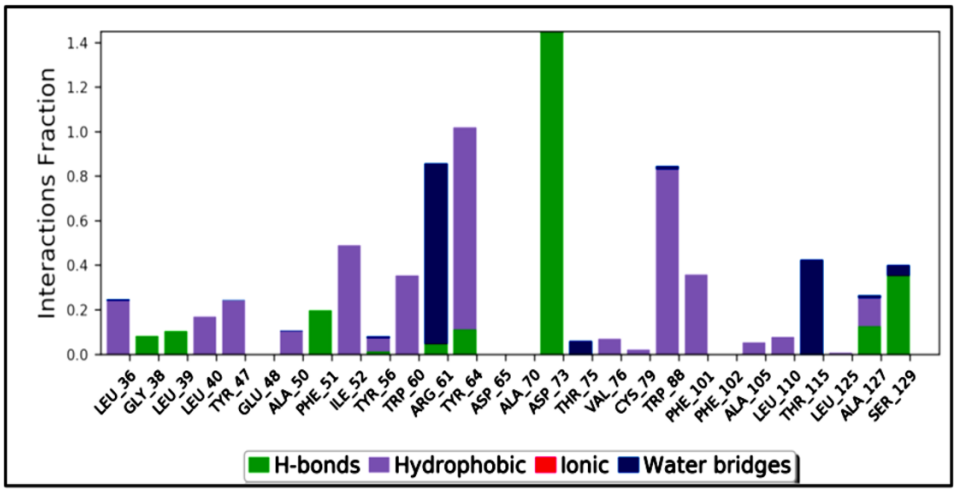

a) LasR-C1 complex

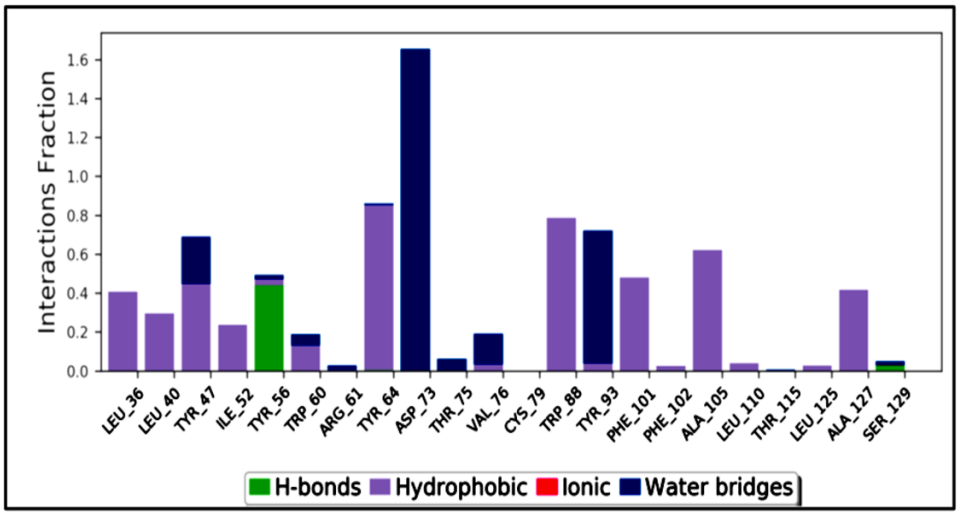

b) LasR-C2 complex

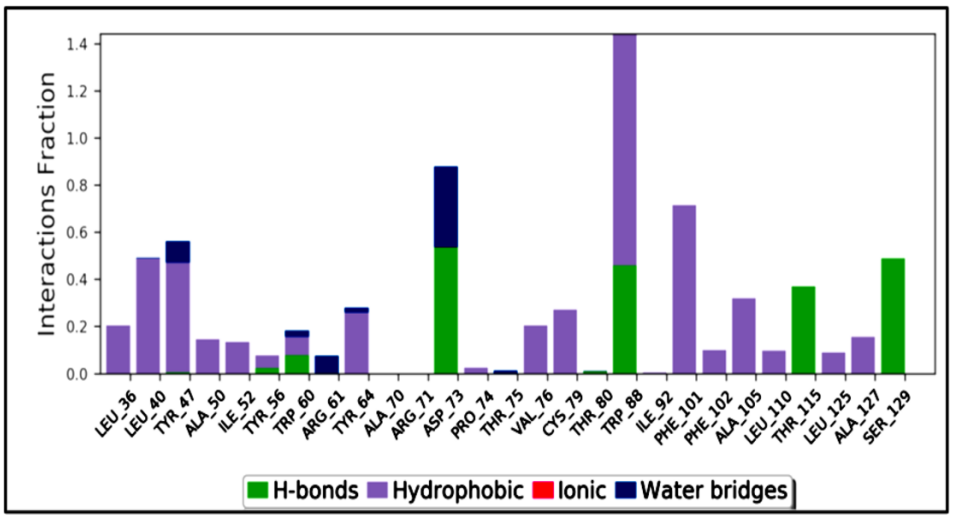

c) LasR-C3 complex

Figure 24

Histogram plots of interaction and type of contacts of selected compounds with LasR

The compound C3 forms hydrogen bonds with amino acids Asp73, Trp88, and Ser129 for more than 40% of the simulation period (Figure 24c). In contradiction, the docked pose of C3 lacked hydrogen bond contact with the protein (Figure 16c). C3 made hydrophobic interactions with the amino acid residues Ala127, Leu125, Leu40, Leu110, Ala105, Phe102, Phe101, Ala50, Leu36, Trp60, Cys79, Ile52, Tyr64, Tyr56, Tyr47, Val76, and Pro74. C3 formed a water bridge with residues Tyr47, Asp73, Trp60, Tyr64, Arg61 and Thr75 for less than 30% of the simulation time (Figure 24c). π-π interactions with residues Phe101 and Trp88 are retained from the docked pose and these interactions are maintained for more than 60% of the simulation process (Plate 2c).

Schiebel *et al.* (2018) stated that strong non-bonded interactions are essential for establishing energetically favorable ligand-protein complexes. Ferreira de Freitas and Schapria, (2017) suggested that potential drugable candidates are typically enriched with hydrophobic interactions to improve their binding stability with the target protein. In line with earlier reports, all three compounds possess good binding stability as they are enriched with hydrophobic contacts in the active pocket residues of LasR.

Among the non-bonded interactions, the hydrogen bond is a crucial component in the drug development process because of its discernible effect on drug selectivity, metabolism, and absorption (Rashid *et al.,* 2022). Müh *et al.* (2006) evidenced that even though both antagonists and agonists bind to the same binding site of LasR, only those lead compounds having hydrogen bond interactions with two amino acids Asp73 and Trp60 could activate LasR. Kim *et al.* (2015) also stated that agonist molecules form hydrogen bonding with Arg61 and Trp60 residues in the LasR active site. It is important to note that selected compounds were not involved in hydrogen bond interaction with Trp60 for a period of 100 ns which further validated the compounds as potent antagonists for LasR.

4.1.5.4. Ligand torsion profile

The ligand torsion profile summarizes the conformation of rotatable bonds in the ligand during the simulation process. The ligand torsion profile helps to understand the conformational stress ligands experience to maintain their protein-bound conformation. In the dial/radial plot, the conformation of the compounds at the beginning of the simulation is marked in the center and changes occuring in each rotatable bond during the simulation are plotted radially outwards (Pourshojaei *et al.,* 2019). The bar plot illustrates the probability

density of each torsion by summarizing the dial plot data. The ligand torsion profile of the compounds are shown in Figure 25-27.

A total of nine rotatable bonds was observed in C1, which are present between ligand atoms: 4 and 10; 10 and 11; 11 and 12; 12 and 13; 13 and 14; 14 and 15; 10 and 21; 24 and 27; and finally between 26 and 28 (Figure 25). In the case of C2, four rotatable bonds are observed between ligand atoms: 13 and 14, 1 and 13, 1 and 9, and 4 and 12 (Figure 26). For the compound C3, eight rotatable bonds (Figure 27) were seen between ligand atoms: 4 and 31; 6 and 7; 12 and 13; 18 and 19; 19 and 20; 20 and 21; 21 and 22; and finally, between 22 and 23. The dial plot and bar chart of C1 showed that rotatable bonds i, ii, iii, iv, vi, and vii were rigid, whereas bonds v, viii, and ix were more flexible. On the other hand, all four bonds exhibited by C2 were rigid in nature. In the case of C3, only one bond (v) was rigid, and all remaining bonds were more flexible.

Pourshojaei *et al.* (2019) have stated that potent inhibitors of protein take up a solid structure that may keep the same binding orientation throughout the simulation, resulting in a narrower band with the least rotational variations. In contrast, the unfavorable ligand moieties exhibit more torsions during the binding process due to weak interactions with active site residues. Jin *et al.* (2020) stated that compounds with fewer rotatable bonds indicate that the molecule had strong rigidity and better binding to the active site. Thus, our findings have shown that the selected compounds C1 and C2 have fewer rotatable bonds and demonstrate their strong binding towards LasR. On the contrary, compound C3 was more flexible and had weaker interaction with LasR.

4.1.5.5. Ligand properties

The stability of the compounds in the active site of LasR during the simulation was determined by analyzing the properties of ligands such as RMSD, radius of gyration (Rg), number of intramolecular hydrogen bonds, molecular surface area (MSA), solvent accessible surface area (SASA), and polar surface area (PSA). The results obtained are provided as a plot in Figure 28-30.

It is observed that the values of the majority of attributes initially fluctuated but eventually became consistent, demonstrating the stability of the compounds in the binding site of the protein. Figure 28 shows that C1 possessed a stable R_g value of 4.7 Å throughout the simulation, which defines the rigid packing of C1 into the LasR active site. No

intramolecular hydrogen bond contacts were seen in C1 throughout the simulation period. SASA was around 30 $Å^2$ up to 80 ns. After that, it was gradually decreased to 20 $Å^2$, which was maintained untill the simulation was complete. MSA and PSA were stabilized around constant values of 400 $Å^2$ and 104 $Å^2$, respectively.

In the case of C2 (Figure 29), the value of R_g was constant at 4.6 Å, which proved its tight packing into the active site of LasR. It also showed no evidence of intramolecular hydrogen bond interactions. The SASA value fluctuated up to 40 ns and later maintained a stable state, with a fixed value of 10 $Å^2$. The MSA and PSA were held constantly at 376 $Å^2$ and 60 $Å^2$, respectively, throughout the simulation period. C3 (Figure 30) exhibited an R_g value of 5.8 Å but there was a slight fluctuation for fewer seconds between 18 and 20 ns, and after that, it again became stable. There were no intramolecular hydrogen bonds in C3. The parameter SASA fluctuated up to 80 ns and remained consistent only after 80 ns around a fixed value of 20 $Å^2$. The properties, namely MSA and PSA, contrary to the other two compounds were found to fluctuate initially and stabilized to values of 464 $Å^2$ and 70 $Å^2$, respectively after 30 ns.

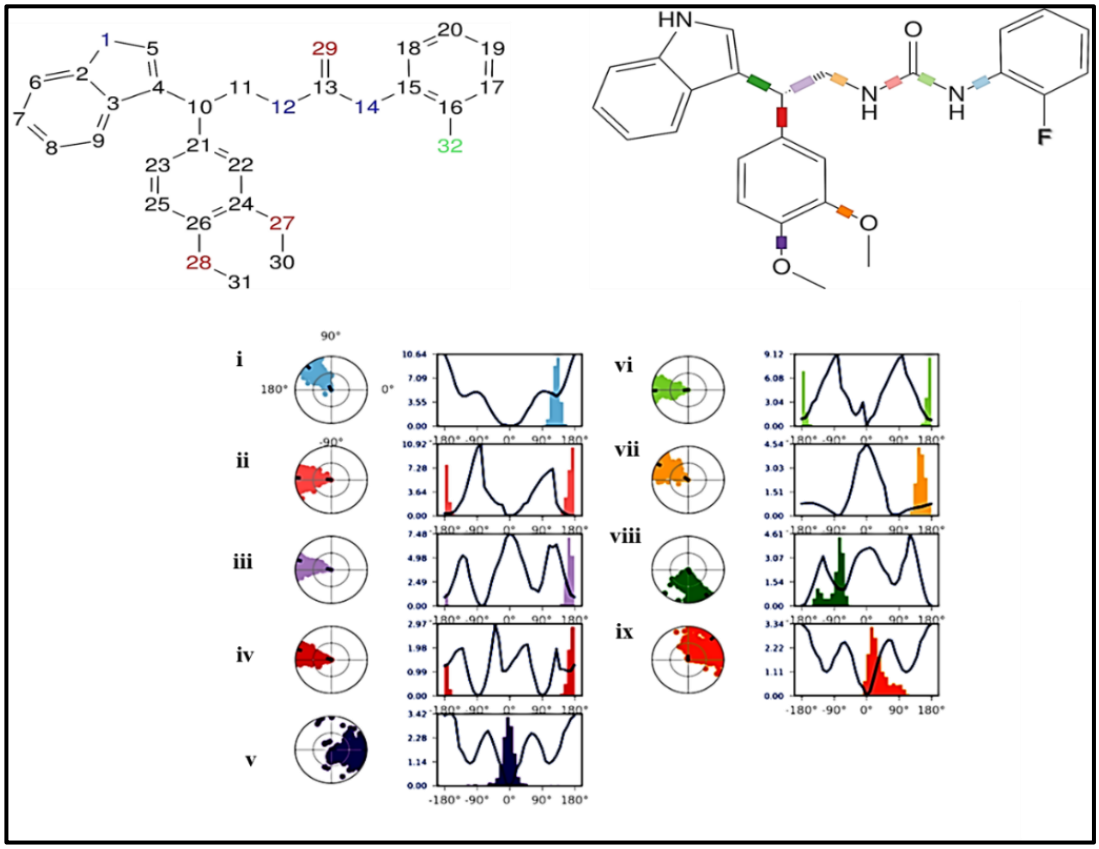

Figure 25
Ligand torsion profile of C1 during simulation

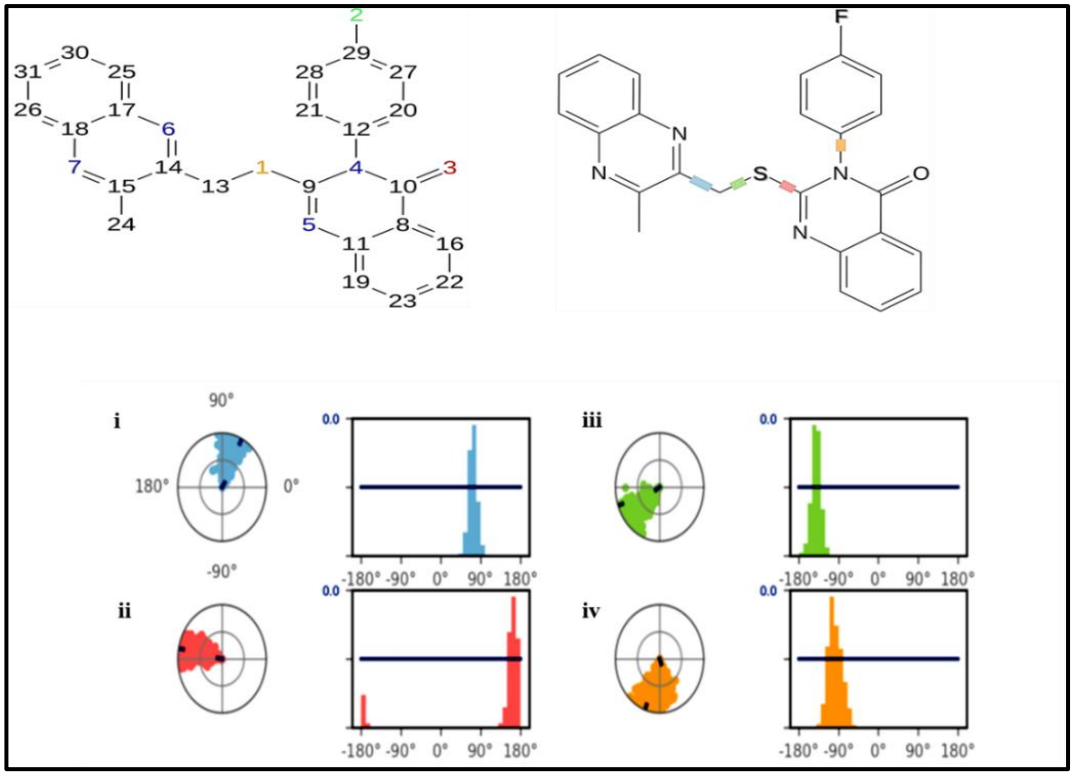

Figure 26
Ligand torsion profile of C2 during simulation

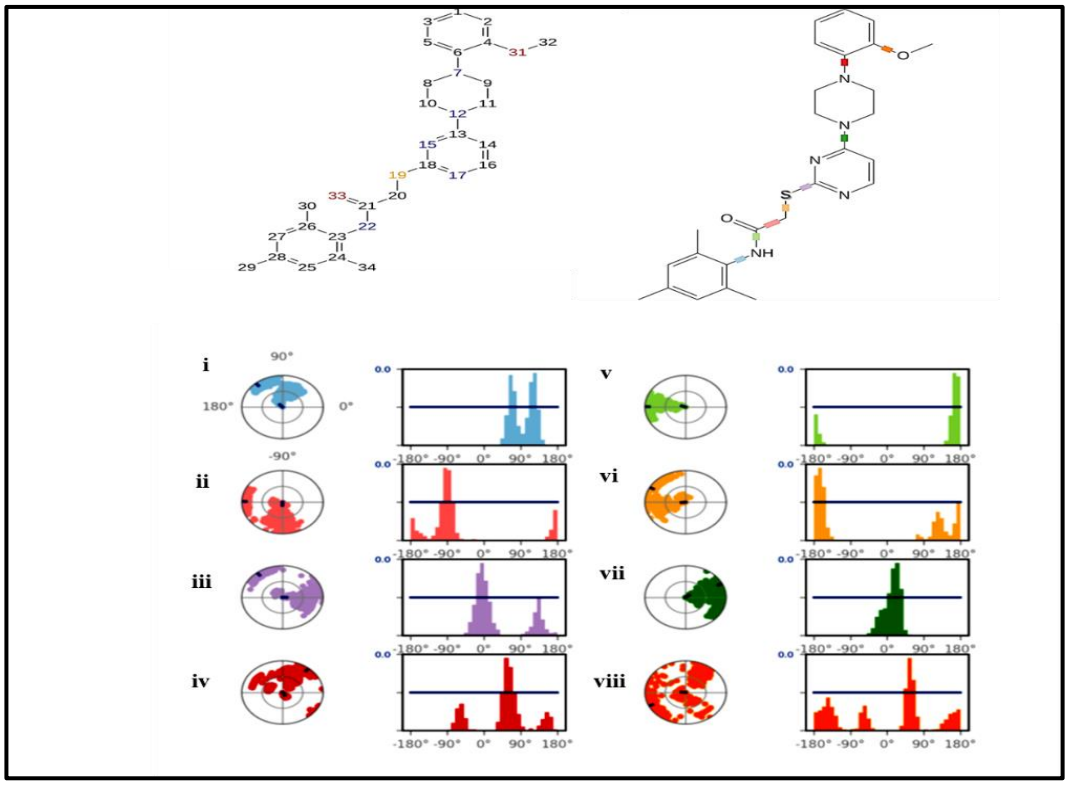

Figure 27
Ligand torsion profile of C3 during simulation

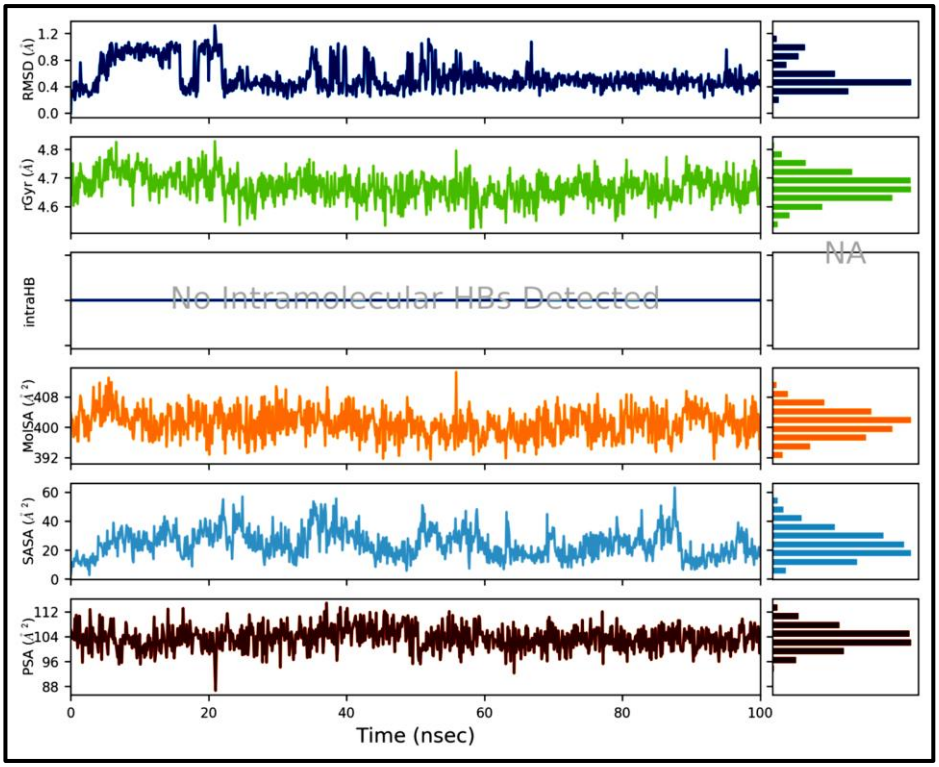

Figure 28
Variations in properties of C1 examined during simulation

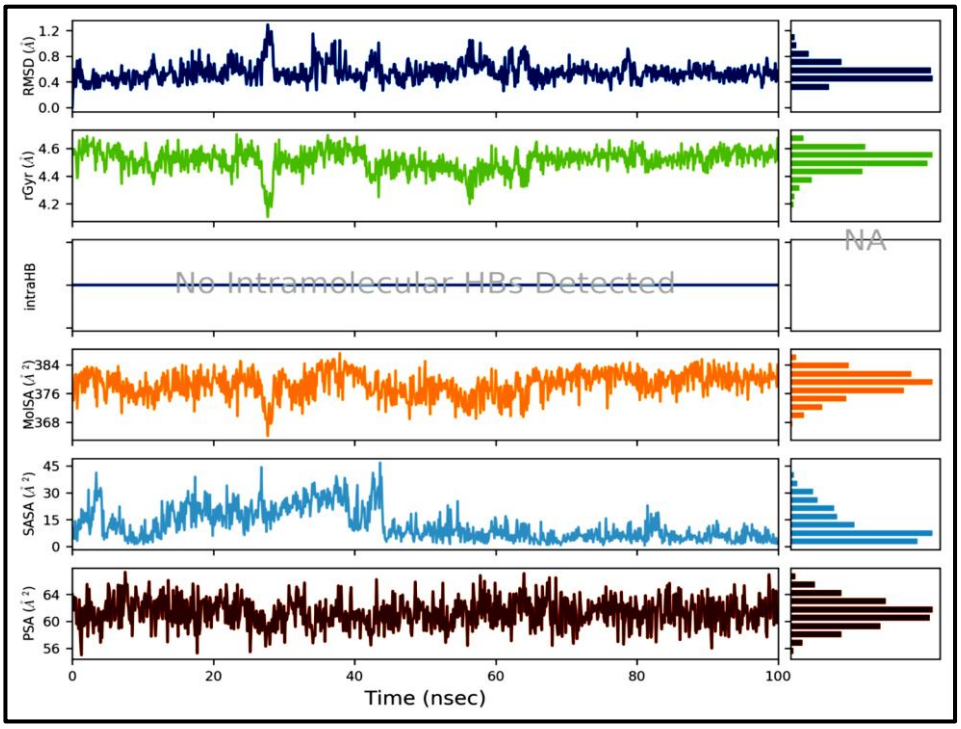

Figure 29
Variations in properties of C2 examined during simulation

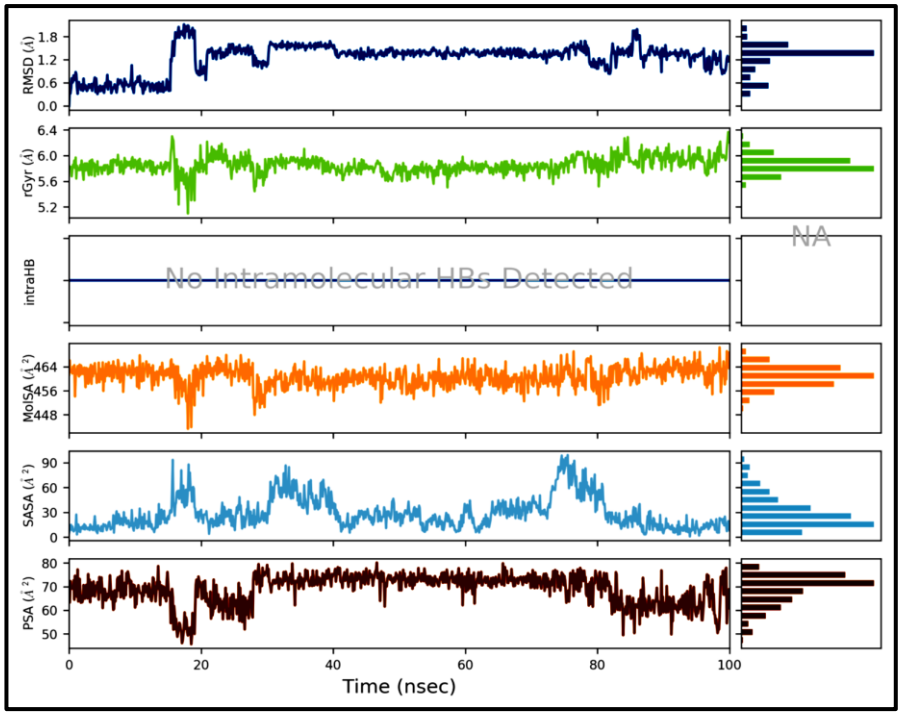

Figure 30
Variations in properties of C3 examined during simulation

In molecular dynamics simulation study, the binding mode and the stability of the selected compounds with LasR were computed using various parameters, including RMSD, RMSF, changes in secondary structure elements, ligand RMSF, protein-ligand interaction profile, ligand torsion profile, and variations in ligand properties over 100 ns simulation. The results portrayed that the three selected compounds possessed better stability, structural conformation, and binding affinity towards LasR. Therefore, the selected compounds can be used as a better lead molecule against LasR for developing an effective antibiofilm agent. Hence, these compounds were purchased and further validated for their antibiofilm and antiquorum sesning activities through *in vitro* studies.

4.1.6. Purchase of compounds

High throughput virtual screening and molecular dynamics analysis revealed that the three compounds C1, C2, and C3 may be considered as potent antagonists for LasR protein of *Pseudomonas aeruginosa.* Further, to validate the compounds for their antibiofilm and antiquorum sensing properties in *in vitro*, the compounds were purchased from Mcule (https://mcule.com/), Hungary and Life Chemicals (https://lifechemicals.com/), Canada.

4.1.7. Cytotoxicity study

Cytotoxicity of the compounds against eukaryotic cells may represent a barrier that eventually limit their utilization in clinical fields. Therefore, to investigate the cytotoxicity of the compounds against mammalian cells, human peripheral blood lymphocyte (PBL) cells were exposed to varying concentrations of compounds and their viability was measured by MTT reduction assay. The obtained results are shown in Figure 31.

Figure 31 revealed that treatment of peripheral blood lymphocyte cells with selected compounds at varying concentrations (125-850 µM) exhibited lesser effects on cell viability, suggesting the lower cytotoxic nature of the compounds. The percentage of viable cells ranged between 70-90% on exposure to different concentrations of compounds. The percent viability of the cell decreased with the increase in the concentration of the compounds.

These findings were in line with the report by Siqueira *et al.* (2021), who stated that silver-complexed sulfonamide, which was effective against *Pseudomonas aeruginosa* biofilms retained cell viability between 70%-90% when tested in human peripheral blood mononuclear cells. Kotzialampou *et al.* (2021) reported that MreB inhibitor A22 hydrochloride showed no cytotoxic effect on human peripheral mononuclear cells.

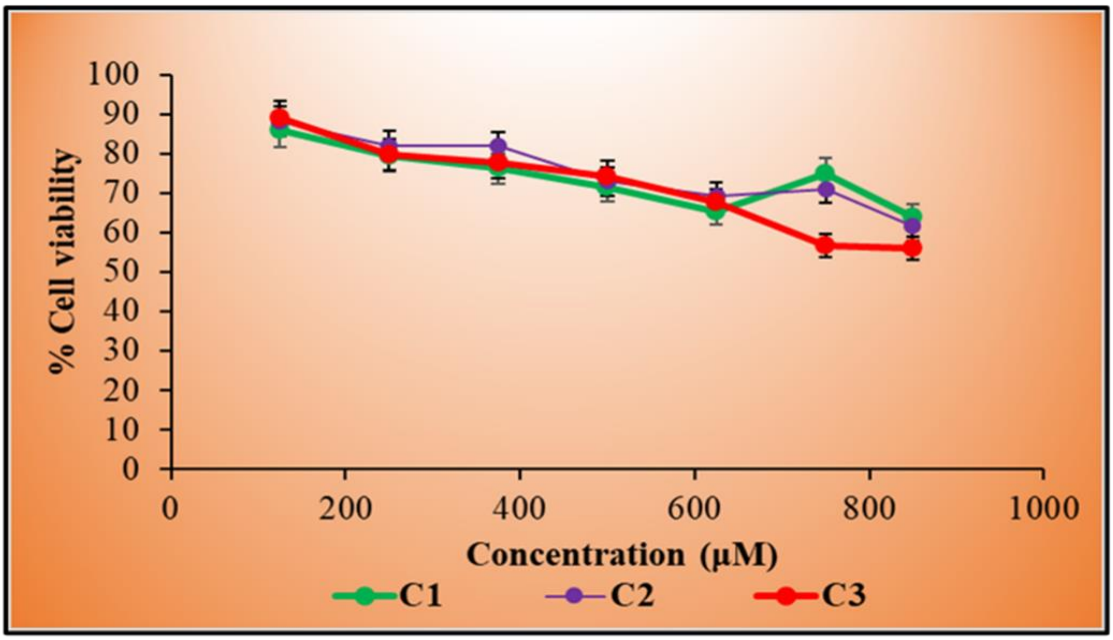

The data represent the mean value of three independent experiments

Figure 31
Evaluation of cytotoxicity of compounds against peripheral blood lymphocyte (PBL) cells

The results of Phase I revealed that three compounds namely CACPD2011a-0001928786 - (3-[2-(3,4-dimethoxyphenyl)-2-(1H-indol-3-yl)ethyl]-1-(2-fluorophenyl)urea) (C1), CACPD2011a-0001927437 - (3-(4-fluorophenyl)-2-[(3-methylquinoxalin-2-yl)methylsulfanyl]quinazolin-4-one) (C2), and CACPD2011a-0000896051 - (2-({4-[4-(2-methoxyphenyl)piperazin-1-yl]pyrimidin-2-yl}sulfanyl)-N-(2,4,6 trimethylphenyl) acetamide) (C3) were chosen based on their highest docking scores in the virtual screening process. All of the three selected compounds were found to possess good pharmacokinetic profile. The selected compounds also demonstrated a stable contact with LasR over the simulation period of 100 ns. In addition, the compounds were found to be non-toxic to human peripheral blood lymphocyte cells, which further paved the way for exploring these compounds for their antibiofilm and antiquorum sensing properties.

4.2. Phase II: Assessment of antibiofilm and antiquorum sensing activity of LasR inhibitors against *Pseudomonas aeruginosa*

4.2.1. Bacterial strains

The wild-type model bacterial strain *Pseudomonas aeruginosa PAO1* (MTCC 2453) and a biomarker strain *Chromobacterium violaceum* (MTCC 2656) were obtained from the Microbial Type Culture Collection and Gene Bank (MTCC), Chandigarh, India. These two strains were used throughout the study to validate the antibiofilm and antiquorum sensing properties of the selected LasR inhibitors. The strains were grown in Luria-Bertani (LB) broth and diluted to an appropriate optical density (OD) before each experiment by measuring their growth in terms of absorbance at 600 nm. The obtained bacterial strains are shown in Plate 3.

4.2.2. Determination of MIC and sub-MIC of selected LasR inhibitors

The minimum inhibitory concentration (MIC) of the selected compounds C1, C2, and C3 against *Pseudomonas aeruginosa PAO1* were identified by the microbroth dilution method. The MIC was observed as the smallest concentration of the compounds that completely retarded the visible bacterial growth in LB broth. The MIC was assessed at a concentration that ranged between 1.95-4000 μM by two-fold serial dilution of the compounds in LB broth. The wells without compounds were taken as growth control. Ciprofloxacin (CP) was reported to have antibiofilm activity against *Pseudomonas aeruginosa* biofilms (Sarkar *et al.*, 2015). Therefore ciprofloxacin, at a sublethal

concentration (0.4 µg/ml), was employed as the positive control for the bioassays. Wells with only medium (LB broth) served as blank, and those with dimethyl sulfoxide (DMSO) were considered as the negative control. The results of the determination of minimum inhibitory concentration are shown in Table 12.

Reference strain: *Pseudomonas aeruginosa PAO1* (MTCC 2453)

Biomarker strain*: Chromobacterium violaceum* (MTCC 2656)

Plate 3
Bacterial strains procured from MTCC

Table 12

Minimum inhibitory concentration of the selected LasR inhibitors

Compounds	Concentrations (µM)											
	4000	2000	1000	500	250	125	62.5	31.25	15.62	7.81	3.9	1.95
C1	-	-	-	+	+	+	+	+	+	+	+	+
C2	-	-	-	+	+	+	+	+	+	+	+	+
C3	-	-	-	-	+	+	+	+	+	+	+	+

"+" indicates presence of growth ; "-" indicates absence of growth

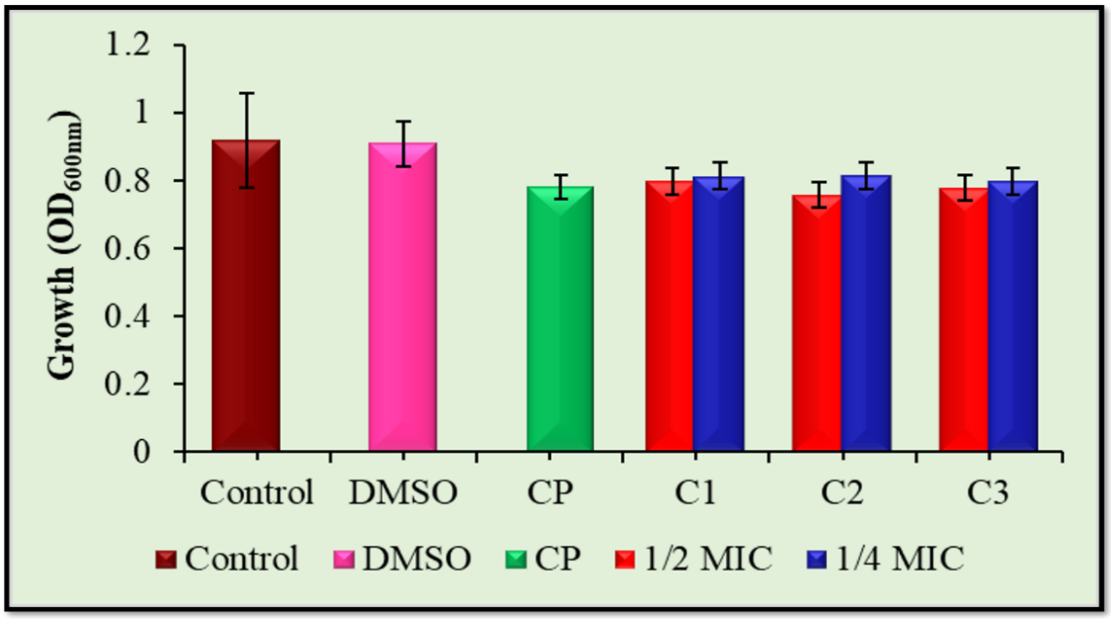

The data represent the mean value of three independent experiments; *p< 0.05, **p <0.01 vs control

Figure 32
Effect of compounds on the growth of *Pseudomonas aeruginosa PAO1*

Table 12 revealed that the MIC was 1000 µM for C1 (43.3 µg/ml) and C2 (42.8 µg/ml), whereas it was 500 µM (23.8 µg/ml) for C3. A concentration range below the MIC value is referred to as sub-MICs of the compounds. In the present study, ½ MIC and ¼ MIC of the compounds were chosen to evaluate the antibiofilm and antiquorum sensing activities. Pattnaik *et al.* (2018) suggested that the most important feature to be considered during the development of any antimicrobial agent is its ability to target the virulence of bacteria rather than killing the bacterial strain. Therefore, to differentiate the antibiotic activity from antiquorum sensing activity, the impact of sub-MICs of the chosen compounds on *Pseudomonas aeruginosa PAO1* growth was analyzed.

The bacteria were incubated in a 96-well microtiter plate with sub-MICs (½ and ¼ MIC) of the selected compounds for 24 hrs. Growth was evaluated by the cloudiness of the media measured at 600 nm. The results (Figure 32) inferred that sub-MICs of the compounds had no significant impact on *Pseudomonas aeruginosa* growth. Therefore, sub-MICs of the compounds were used in subsequent studies.

Majumdar *et al.* (2020) identified the MIC of andrograpanin (0.832 mM), a secondary metabolite found in the leaves of *Andrographis paniculata* against *Pseudomonas aeruginosa* using the microdilution method. They further stated that there was no discernible change in bacterial cells when treated with sub-MIC level of the compound. The MIC

of *Pestalotiopsis sydowiana* fungal extract against *Pseudomonas aeruginosa PAO1* was determined to be 1000 µg/ml and their sub-MICs lacked a significant impact on *Pseudomonas aeruginosa PAO1* growth (Parasuraman *et al.,* 2020).

Walczak *et al.* (2021) reported that the MIC of carvacrol, an essential oil extracted from *Origaneum vulgare* against *Pseudomonas aeruginosa PAO1* was found to be 1 mg/10 µl, and their sub-MICs when tested, did not have any direct bactericidal effects on the test pathogen. Pattnaik *et al.* (2018) stated that the MIC of a fungal extract of *Diaporthe phaseolorum SSP12* against *Pseudomonas aeruginosa PAO1* was observed to be 1000 µg/ml.

4.2.3. Assessment of antibiofilm activity

4.2.3.1. Biofilm inhibition

Biofilm formation is a crucial defense mechanism that aids in developing bacterial pathogenicity in host cells. The structural architecture of *Pseudomonas aeruginosa* biofilms is highly complex and serves as a diffusion barrier by slowing the pace at which the antibiotics are absorbed, avoiding an excessive build-up of drugs, and giving time for the production of resistance genes (Ahmed *et al.,* 2019).

The topological changes such as cell-cell communications, EPS overproduction, extracellular fibrillar networks, pellicles, multiple layers, and microcolony may contribute to stable biofilm states (Kamali *et al.,* 2020). Crystal violet staining assay was performed to identify the impact of selected compounds on development of biofilm by *Pseudomonas aeruginosa PAO1*. The results obtained are depicted in Figure 33.

The compounds were able to prevent the formation of biofilm to about more than 50%. The percentage of biofilm inhibition by C1 at ½ MIC and ¼ MIC was found to be 85% and 81% respectively. At ½ MIC, C2 and C3 attenuated the biofilm development up to 84% and 83% respectively. The compounds C2 and C3 at ¼ MIC, arrested the biofilm development up to 81% and 82% respectively. The antibiofilm activity of the compounds used in the present study was comparable to ciprofloxacin (87%).

These results were in line with earlier reports where Zhong *et al.* (2020) reported three natural compounds butein, catechin-7-xyloside, and sappanol at 100 µM inhibited biofilm of *Pseudomonas aeruginosa* up to 72.45%, 66%, and 54.26%, respectively. Parasuraman *et al.* (2020) demonstrated that crude fungal extract of *Pestalotiopsis sydowiana*

reduced *Pseudomonas aeruginosa PAO1* strain biofilms to 54% and 72% at 250 µg/ml and 500 µg/ml, respectively.

Khan *et al.* (2021) also documented that gold and zinc oxide nanoparticles of phloroglucinol extract effectively reduced the biofilm forming potency of *Pseudomonas aeruginosa PAO1* strain in a dose dependent way. Baloyi *et al.* (2021) observed that methanolic extract of *Melianthus comosus (Vahl)* arrested formation of biofilm in a concentration dependent manner. Walczak *et al.* (2021) reported that inhibition of *Pseudomonas aeruginosa* biofilms by thymol and carvacrol occurred dose-dependently. The findings were in line with the above literatures where the compounds C1, C2, and C3 arrested the biofilm in a dose-dependent manner in *Pseudomonas aeruginosa PAO1*.

4.2.3.2. Eradication of preformed matured biofilm

Disruption of preformed matured biofilm is an important characteristic as it prevents dispersion of biofilms. The disruption ability of the selected compounds at sub-MICs on preformed matured biofilm of *Pseudomonas aeruginosa PAO1* was evaluated by the crystal violet staining method. The free-floating cells from the developed biofilm were discarded after 24 hrs of incubation, and the attached cells were incubated with fresh LB broth containing sub-MICs of compounds. The obtained results are provided in Figure 34.

It was revealed that the compounds possessed a higher potential to disrupt preformed matured biofilms of *Pseudomonas aeruginosa PAO1* on exposure to their sub-MIC doses. The percentage of biofilm disruption was 84%, 75%, and 81% for the ½ MIC of compounds C1, C2, and C3, respectively. At ¼ MIC level, C1, C2, and C3 showed a percentage of biofilm disruption up to 78%, 74%, and 76%, respectively. The compounds showed a dose-dependent potential to destroy the preformed matured *Pseudomonas aeruginosa PAO1* biofilms. Ciprofloxacin exhibited an eradication percentage of 86%. The highest disruption ability was demonstrated by C1 (84%) at ½ MIC, and the lowest was by C2 (74%) at ¼ MIC.

The results corroborates with the results of Khan *et al.* (2019), wherein artificially synthesized chitosan-polypyrrole nanocomposites disrupted matured biofilm of *Pseudomonas aeruginosa PAO1* in a dose-dependent manner. Khan *et al.* (2021) also stated that gold and zinc oxide nanoparticles of phloroglucinol disrupted up to 68% and 60% of grown biofilms of *Pseudomonas aeruginosa PAO1,* respectively at 1024 µg/ml.

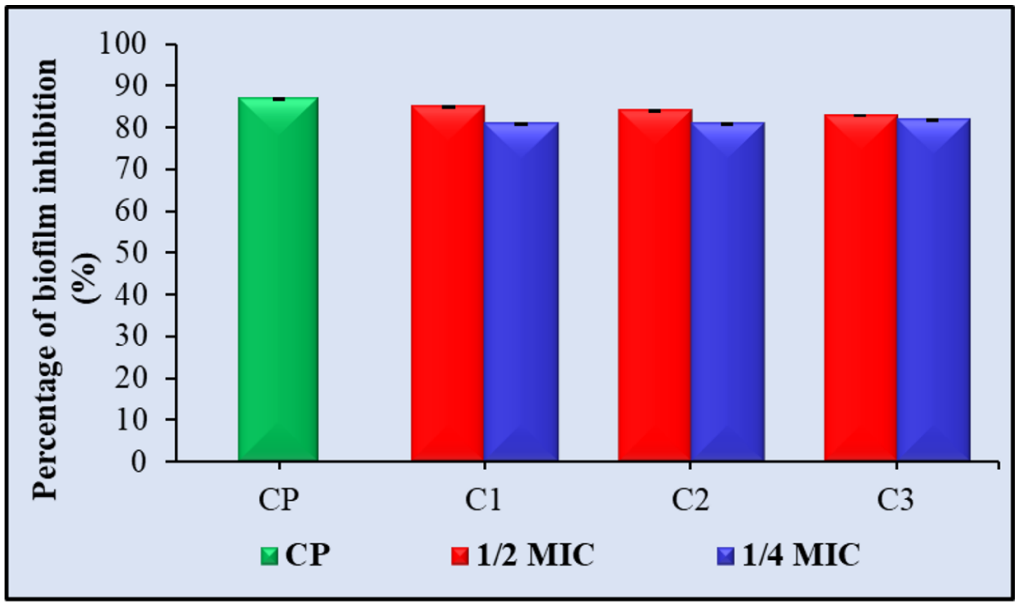

Values represented indicate percent reduction in biofilm formation over control
The data represent the mean value of three independent experiments

Figure 33

Effect of compounds on biofilm formation in *Pseudomonas aeruginosa PAO1*

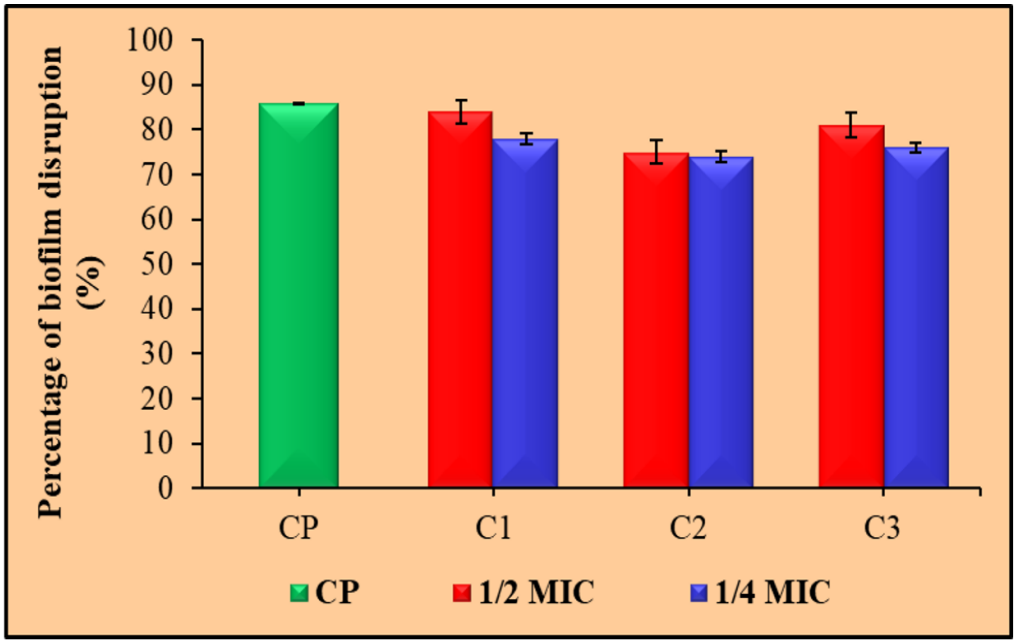

Values represented indicate percent disruption of biofilm over control
The data represent the mean value of three independent experiments

Figure 34

Effect of compounds on preformed matured biofilm of *Pseudomonas aeruginosa PAO1*

4.2.3.3. Exopolysaccharide production

The adhesion ability and persistence of biofilm are well associated with the structured matrix consisting of exopolysaccharides (EPS), proteins, and lipids as they block the invasion of antimicrobial agents and antimicrobial peptides into cells by serving as a protective shield. Mainly, EPS accounts for the more significant portion of the dry mass of biofilm and leads to the diminished potency of most antibiotics (Karigianni *et al.,* 2020).

Quorum sensing-based EPS secretion is thought to be more crucial for preserving the structural integrity of the biofilm and is also known to impact microcolony formation in *Pseudomonas aeruginosa*. A decrease in EPS production may enhance antibiotic activity by improving drug penetration and thereby arresting progression in biofilm formation, disruption of biofilm structure, and demolition of entrapped bacterial cells (Fu *et al.,* 2021). Therefore, the impact of selected compounds on EPS production in *Pseudomonas aeruginosa* was determined using the phenol-sulphuric acid method. The EPS production is expressed as absorbance at 490 nm, and the results are provided in Table 13.

On comparison with control (0.71 ± 0.12), the tested compounds C1, C2, and C3 at ½ MIC significantly ($p<0.01$) reduced the absorbance at 490 nm to 0.21 ± 0.01, 0.23 ± 0.008, and 0.23 ± 0.02, respectively. In presence of inhibitors C1, C2, and C3 at ¼ MIC, the optical density was significantly ($p<0.01$) reduced to 0.29 ± 0.002, 0.34 ± 0.03, and 0.29 ± 0.05, respectively, compared to the untreated control.

The percentage reduction in EPS was found to be 70%, 67%, and 68% at ½ MIC of C1, C2, and C3, respectively. Treatment with ¼ MIC dose of C1, C2, and C3 also effectively decreased EPS production to 59%, 52%, and 59%, respectively. The maximum attenuation of EPS was found at ½ MIC of C1 (70%), which was comparable to the positive control ciprofloxacin (70%).

These findings were in concordance with the earlier observation of Razdan *et al.* (2022), wherein EPS production in *Pseudomonas aeruginosa* was decreased on treatment with clove oil loaded with levofloxacin. Sagar *et al.* (2022) stated that the methanolic extract of *Eucalyptus globulus* had a maximum inhibitory effect of 53% on the synthesis of EPS in *Pseudomonas aeruginosa PAO1*.

Chatterjee *et al.* (2021) indicated that cuminaldehyde drastically declined the amount of EPS produced by *Pseudomonas aeruginosa* with a maximum attenuation of 40% at

60 µg/ml. Ismail *et al.* (2021) also documented a significant arrest in the EPS production in *Pseudomonas aeruginosa* up to 75% in presence of *Callistemon citrinus* extract (500 µg/ml).

Table 13
Effect of compounds on EPS production in *Pseudomonas aeruginosa PAO1*

S.No	Treatment	Concentration	EPS production (OD_{490})
1	Untreated Control	-	0.71 ± 0.12
2	DMSO	-	0.67 ± 0.06
3	Ciprofloxacin	½ MIC	0.21 ± 0.01** (70%)
4	C1	½ MIC	0.21 ± 0.01** (70%)
		¼ MIC	0.29 ± 0.002** (59%)
5	C2	½ MIC	0.23 ± 0.008** (67%)
		¼ MIC	0.34 ± 0.03** (52%)
6	C3	½ MIC	0.23 ± 0.02** (68%)
		¼ MIC	0.29 ± 0.05** (59%)

Values in parentheses indicate percent reduction in EPS production over control
The data represent the mean value of three independent experiments; *p<0.05, **p<0.01

4.2.3.4. Alginate production

The alginate production in *Pseudomonas aeruginosa PAO1* is mediated through *rhl* QS system and holds a predominant role in the development of biofilms, protecting bacteria from adverse environmental conditions in hosts. Alginate assist bacteria in evading the alveolar macrophage of the host immune system. Moreover, alginate overexpressing *Pseudomonas aeruginosa* strains were isolated from chronic lung infection patients (Zhao *et al.*, 2022). Hence, the effectiveness of selected compounds on the production of alginate was assessed, and the results are given in Table 14.

The alginate production was expressed as absorbance at 530 nm. In untreated control, the absorbance was 0.85 ± 0.05. It was seen that the compounds significantly ($p<0.01$) decreased the absorbance at 530 nm when exposed to their different sub-MIC dosages. In the presence of ciprofloxacin, alginate production was retarded by up to 62%. The percentage of inhibition of alginate production observed at ½ MIC of C1, C2, and C3 were 64%, 60%, and 54%, respectively. On treatment with ¼ MIC, the percent reduction was found to be 46% for all three compounds. The highest inhibition of alginate production was observed at ½ MIC

of C1 (64%), followed by C2 (60%) and C3 (54%). The antibiotic ciprofloxacin reduced the alginate production to 62%.

These results concord with the observations of Tao *et al.* (2022), who stated that *Potentilla kleiniana Wight* suppressed alginate production in *Pseudomonas aeruginosa PAO1* in a dose-dependent manner. Similarly, Pattnaik *et al.* (2018) also said that *Diaporthe phaseolorum SSP12* fungal extract showed a concentration-dependent decrease in alginate production whose inhibition percentage was found to be 48%, 72%, and 84% at sub-MIC doses of 250, 500, and 750 µg/ml, respectively. Dahibhate *et al.* (2022) described that bioactive fraction of *Bruguiera gymnorhiza* at 16 µg/mL resulted in a 51% decline in alginate production.

4.2.3.5. Biofilm total protein production

The matrix material of biofilms comprises of exopolysaccharides, proteins, lipids, and DNA molecules that aid in structural stability. The concentration of extractable protein in a biofilm is proportional to the number of bacteria present (Zhao *et al.*, 2022). The amount of extractable protein in *Pseudomonas aeruginosa PAO1* biofilms was measured according to Lowry's method. The results obtained are depicted in Figure 35.

Upon treatment with compounds C1, C2, and C3 at ½ MIC, the amount of extractable protein in biofilm was reduced to 99.65 µg/ml, 112.43 µg/ml, and 112.04 µg/ml, respectively compared to the control (261.73 µg/ml). In the presence of ¼ MIC of C1, C2, and C3, the protein concentration in biofilm was reduced to 109.43 µg/ml, 129.77 µg/ml, and 134.99 µg/ml, respectively.

The amount of protein in biofilms was decreased on treatment with sub-MIC doses of C1 followed by C2 and C3. The total protein concentration in *Pseudomonas aeruginosa PAO1* biofilm treated with ciprofloxacin was 97.31 µg/ml. Consistent with our findings, Chatterjee *et al.* (2021) reported that a cuminaldehyde treated *Pseudomonas aeruginosa* biofilms showed a significantly lower protein level than the control with a maximum protein inhibition rate of 38% (60 µg/ml). Bose *et al.* (2020) stated that nano encapsulated α-terpineol decreased the amount of protein in *Pseudomonas aeruginosa* biofilms to 72%.

Table 14

Effect of compounds on alginate production in *Pseudomonas aeruginosa PAO1*

S.No	Treatment	Concentration	Alginate production (OD_{530})
1	Untreated Control	-	0.85 ± 0.05
2	DMSO	-	0.80 ± 0.01
3	Ciprofloxacin	½ MIC	0.32 ± 0.05** (62%)
4	C1	½ MIC	0.31 ± 0.03* (64%)
		¼ MIC	0.46 ± 0.10** (46%)
5	C2	½ MIC	0.34 ± 0.11** (60%)
		¼ MIC	0.46 ± 0.09** (46%)
6	C3	½ MIC	0.39 ± 0.05** (54%)
		¼ MIC	0.46 ± 0.14** (46%)

Values in parentheses indicate percent reduction in alginate production over control
The data represent the mean value of three independent experiments; *p<0.05, **p<0.01

4.2.4. Evaluation of metabolic activity of viable cells in biofilm

4.2.4.1. MTT reduction assay

Biofilms consist of subpopulations of cells that are metabolically active and non-active. These subpopulations exhibit various altered phenotypes on exposure to antibiotics. Most antibiotics work well in metabolically active cells. The metabolically inactive cells exhibit lower susceptibility to antibiotics. As a result, they develop resistance to conventional antibiotics, which aid in bacterial pathogenesis in the hosts (Majumdar *et al.,* 2020). MTT assay was used to validate bacterial cell viability in biofilm after treatment with compounds, and the obtained results are shown in Figure 36.

The percentage of metabolically active cells in biofilm was found to be 40%, 45%, and 45% after treatment with ½ MIC of C1, C2, and C3, respectively. The percentage of viable biofilm cells increased at a lower concentration of ¼ MIC of compounds. C1 markedly decreased the number of active biofilm cells compared to other two compounds. The positive control ciprofloxacin showed a percentage of cell viability of 40%, which was comparable to that of C1.

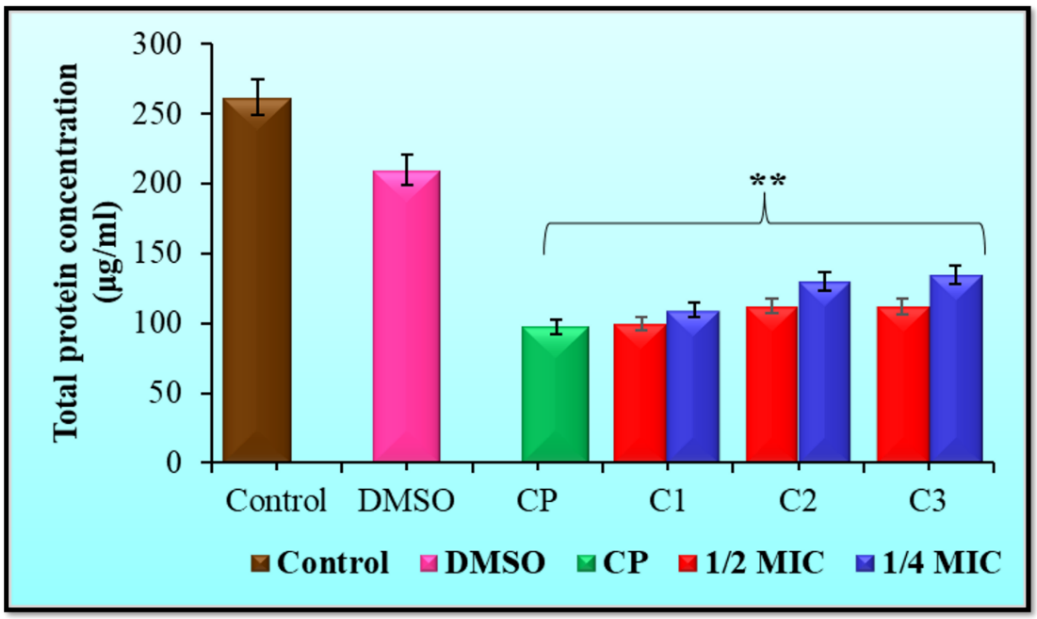

The data represent the mean value of three independent experiments; *p< 0.05, **p <0.01 vs control

Figure 35

Effect of compounds on total protein concentration in *Pseudomonas aeruginosa PAO1* biofilm

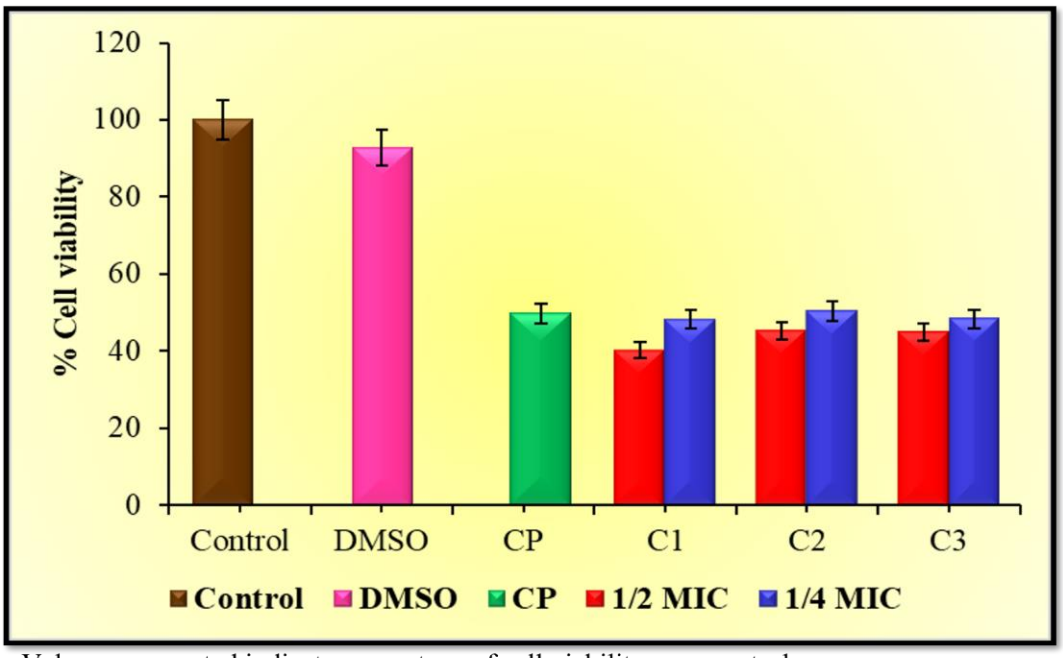

Values represented indicate percentage of cell viability over control
The data represent the mean value of three independent experiments

Figure 36

Effect of compounds on viability of *Pseudomonas aeruginosa PAO1* biofilm cells

Overall, the results revealed that bacterial cell viability was drastically decreased compared to control on treatment with all three compounds. Hence, the results of the present study suggested that these compounds could probably reduce the amount of biofilm formed by *Pseudomonas aeruginosa PAO1* by distinctly hampering the biofilm-forming cells. In concordance with these results, Parai *et al.* (2018) stated that reserpine at their sub-MIC doses reduced the metabolically active cells in *Pseudomonas aeruginosa PAO1* biofilm to 59% and 38%.

Dey *et al.* (2020) reported a significant decline in the active biofilm cells to 14% and 30% upon treatment with naringin in combination with ciprofloxacin and tetracycline, respectively in *Pseudomonas aeruginosa PAO1*. Martinez *et al.* (2019) stated that there was a loss in bacterial cell viability, with the proportion of dead cells raised to about ~90% when treated with antimicrobial peptide P5 against *Pseudomonas aeruginosa.*

4.2.5. Assessment of antiquorum sensing activity

4.2.5.1. Violacein inhibition in *Chromobacterium violaceum*

The antiquorum sensing activity was assessed by evaluating the effect of compounds on QS-regulated production of violacein in the QS biomarker strain *Chromobacterium violaceum* (MTCC 2656). Violacein is a purple pigment whose synthesis is regulated by a LuxR homolog, CViR in *Chromobacterium violaceum* (Singh *et al.,* 2017). Antiquorum sensing activity of the selected compounds was assessed using the agar well diffusion assay and the results obtained are presented in Plate 4.

The presence of a creamy white halo around the well against the purple lawn of bacteria indicates the antiquorum sensing activity. The translucent zone indicates inhibition of bacterial growth. The colourless zone of inhibition around the compound-treated wells was found to be opaque (Plate 4), indicating that halos are due to the quorum sensing inhibition and not due to the inhibition of bacterial growth. The diameter (in mm) of the opaque halo zones was measured and given in Table 15.

Table 15 revealed that the zone of violacein inhibition of the compounds ranged from 10.3 ± 0.04 mm to 15 ± 0.08 mm at ½ MICs. The violacein inhibition achieved for the C1, C2, and C3 at ½ MICs were 14.6 ± 0.04, 15.0 ± 0.08, and 10.3 ± 0.04, respectively. The mean violacein inhibition zone of C1 and C2 at ¼ MICs were 11.66 ± 0.47 mm and 7.0 ± 0 mm, respectively. It is also noted that C3 at ¼ MIC did not exhibit any inhibitory

effect on violacein production. The zone of violacein inhibition of ciprofloxacin was measured as 13.0 ± 0 mm.

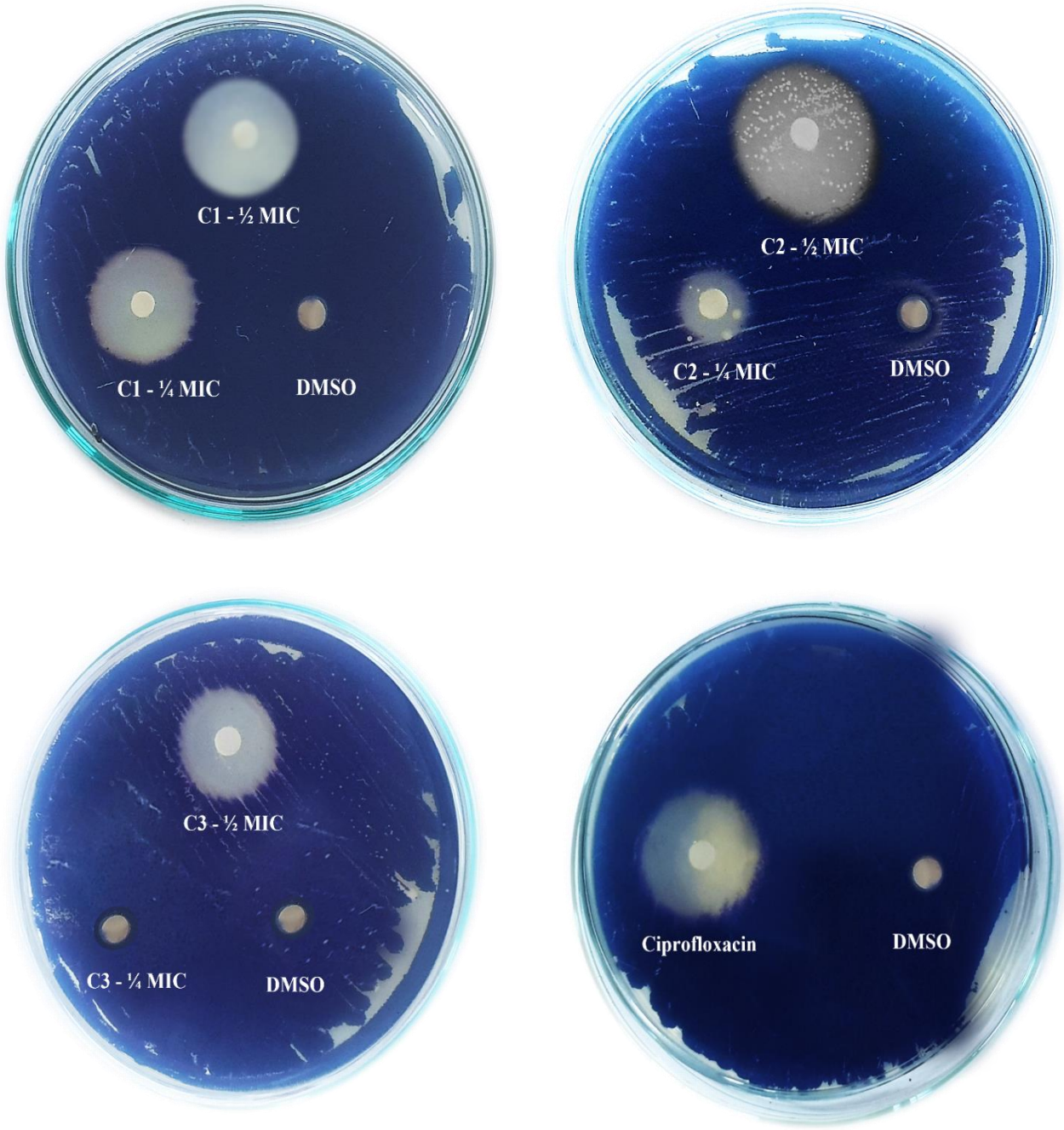

Plate 4

Analysis of antiquorum sensing activity of compounds in *Chromobacterium violaceum*

Table 15

Effect of compounds on violacein pigment production in *Chromobacterium violaceum*

S. No	Treatment	Concentration	Diameter of zone of inhibition (mm)
1	DMSO	-	Nil
2	Ciprofloxacin	½ MIC	13.0 ± 0
3	C1	½ MIC	14.6 ± 0.04
		¼ MIC	11.7 ± 0.47
4	C2	½ MIC	15.0 ± 0.08
		¼ MIC	7.0 ± 0
5	C3	½ MIC	10.3 ± 0.04
		¼ MIC	-

The data represent the mean value of three independent experiments

Ravichandran *et al.* (2018) observed that the QS mechanism in *Chromobacterium violaceum* was inhibited by QSIs of *Pseudomonas aeruginosa*, namely catechin 7-xyloside, sappanol, and butein. Anju *et al.* (2022) reported that hispidulin at 75 µg/mL showed maximum inhibition on production of violacein pigment up to 72% in *Chromobacterium violaceum.* The previous reports by Wang *et al.* (2019) also suggested that compounds having the ability to inhibit the violacein pigment production without affecting the growth of *Chromobacterium violaceum* will be promising quorum sensing inhibitors.

4.2.5.2. Swimming motility

The formation and evolution of biofilms invariably begin with adherence and colonization which are regulated by flagellar motilities, and later, by twitching motility. The motility of a bacteria is vital for biofilm formation, as the bacteria get adhered to a surface or substratum by the process of these flagella-driven motilities that spread out through swimming and swarming (Singh *et al.*, 2017).

Previous reports have suggested that the downregulation of motility leads to a decrease in the severity of pathogenesis and would directly impact development of biofilm in *Pseudomonas aeruginosa* (Zhou *et al.*, 2021; El-Mowafy *et al.*, 2014; Gutierrez *et al.*, 2013). Therefore, the influence of inhibitors on the motility behaviour of

Pseudomonas aeruginosa PAO1 was observed to validate its antiquorum sensing properties further. The diameter of the migration zone (mm) was calculated after 24 hrs and shown in Table 16 and Plate 5.

Table 16
Diameter of swimming motility zone exhibited by *Pseudomonas aeruginosa PAO1* in treated and untreated conditions

S. No	Treatment	Concentration	Diameter of swimming zone (mm)
1	Untreated Control	-	41.3 ± 0.57
2	DMSO	-	38.7 ± 1.15
3	Ciprofloxacin	½ MIC	36.5 ± 0.50*
4	C1	½ MIC	33.0 ± 1.0**
		¼ MIC	34.8 ± 0.76**
5	C2	½ MIC	33.6 ± 0.57**
		¼ MIC	37.6 ± 0.57**
6	C3	½ MIC	33.6 ± 0.52**
		¼ MIC	35.6 ± 0.57*

The data represent the mean value of three independent experiments; *p<0.05, **p<0.01

The untreated *Pseudomonas aeruginosa PAO1* was able to migrate and proliferate to a colony diameter of 41.3 ± 0.57 mm. Compounds C1, C2, and C3 at ½ MIC were able to reduce the colony diameter to 33 ± 1.0 mm, 33.6 ± 0.57 mm, and 33.6 ± 0.52 mm, respectively. The colony diameter was 34.8 ± 0.76 mm, 37.6 ± 0.57 mm, and 35.6 ± 0.57 mm on treatment with compounds C1, C2, and C3, respectively, at ¼ MICs. The swimming motility of *Pseudomonas aeruginosa PAO1* was shrunk by 19-20% and 9-16% on treatment with compounds at ½ and ¼ MICs, respectively. In the presence of ciprofloxacin, the swimming motility zone of *Pseudomonas aeruginosa PAO1* was observed to be 36.5 ± 0.50 mm.

Previous studies have shown that bioactive fraction of *Cassia fistula* (Peerzada *et al.,* 2022), ginkgolic acid (Suo *et al.,* 2022), *Coridothymus capitatus* essential oil (Vrenna *et al.,* 2021), epigallocatechin-3-gallate (Hao *et al.,* 2021), and chitosan-polypyrrole nanocomposites (Khan *et al.,* 2019) were able to reduce the swimming motility of *Pseudomonas aeruginosa PAO1* strain. The findings of the present study are on par with the above literature.

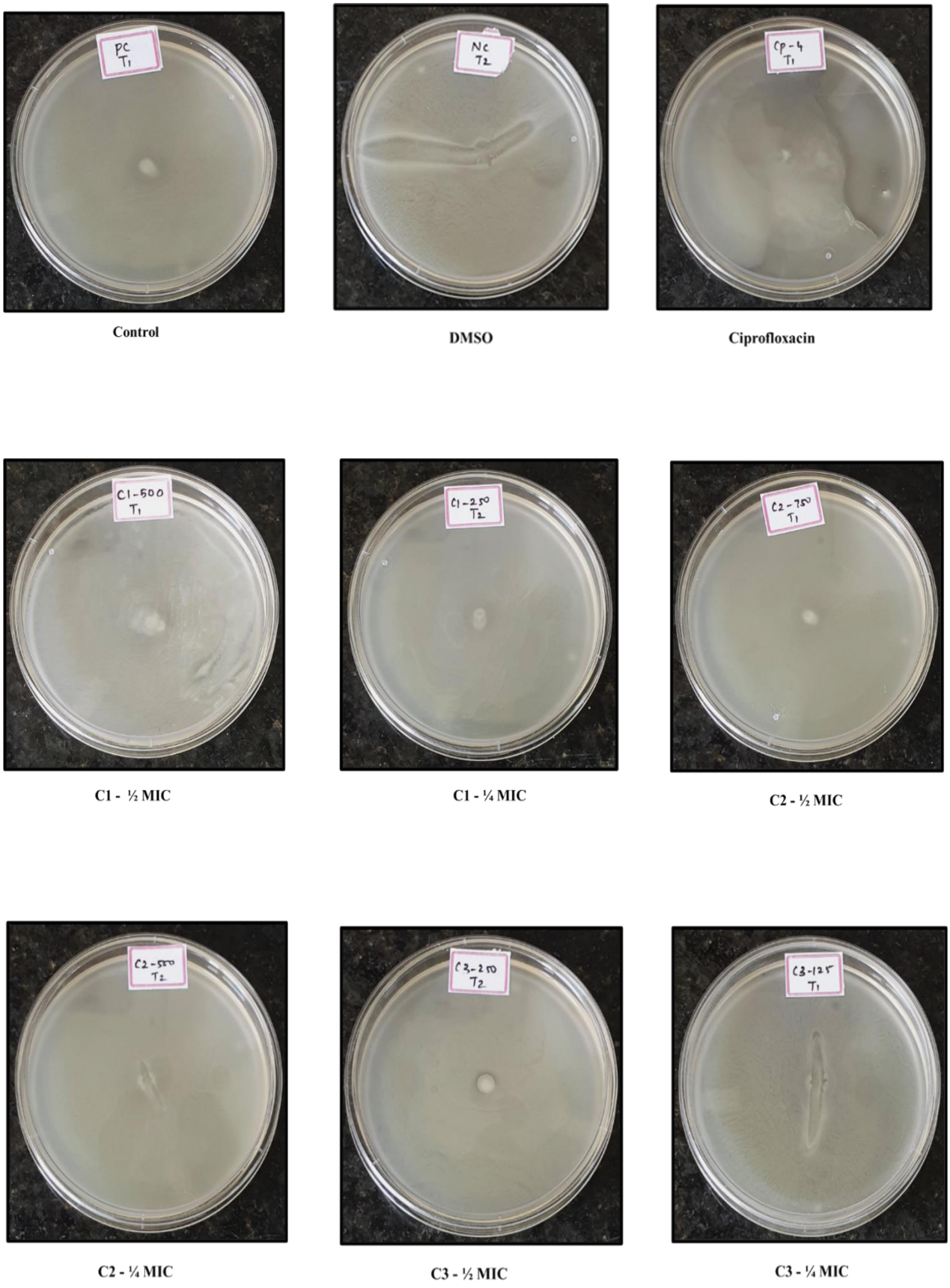

Control | DMSO | Ciprofloxacin

C1 - ½ MIC | C1 - ¼ MIC | C2 - ½ MIC

C2 - ¼ MIC | C3 - ½ MIC | C3 - ¼ MIC

Plate 5
Effect of compounds on swimming motility of *Pseudomonas aeruginosa PAO1*

4.2.5.3. Swarming motility

Swarming motility is a form of flagella-mediated movement that aids in surface adhesion and biofilm development by facilitating cells to colonize an environment rich in nutrients. The bacterial translocation occurs rapidly when numerous well-organized colonies move across a substrate through swarming motility.

Inhibition of bacterial motility would negatively contribute to biofilm formation by modulating the gene expression essential for producing flagella and preventing stable assembly of type IV pili on the surface (Alhajlan *et al.,* 2013). Hence, the impact of compounds on suppressing the flagellum-driven swarming of *Pseudomonas aeruginosa PAO1* was investigated. The decrease in the swarming migration was noted after 24 hrs by measuring the swarm zone (mm) of *Pseudomonas aeruginosa PAO1*. The results are depicted in Table 17 and Plate 6.

The compounds C1, C2, and C3 at ½ MIC minimized the diameter of the swarm zone from 37.6 ± 0.57 mm in untreated control to 4.8 ± 0.28 mm, 5.6 ± 0.57 mm, and 6.5 ± 0.50 mm, respectively. The colony diameter of *Pseudomonas aeruginosa PAO1* at ¼ MIC of compounds was recorded as 6.6 ± 0.57 mm (C1), 6.6 ± 1.85 mm (C2), and 7.3 ± 0.57 mm(C3). The present study reveals that C1 had a maximum inhibitory effect on swarming motility, followed by C2 and C3 in a concentration-dependent manner. The positive control ciprofloxacin significantly ($p<0.01$) reduced the swarm zone of *Pseudomonas aeruginosa PAO1* to 2.8 ± 0.25 mm.

These results revealed that the chosen compounds profoundly affect swarming motility compared to swimming motility. The positive control ciprofloxacin has also shown a similar pattern of inhibition of motility in *Pseudomonas aeruginosa PAO1.* The results are in line with the earlier studies of antiquorum sensing activity of naringin (Dey *et al.,* 2020) and baicalin (Luo *et al.,* 2017). The flavonoids baicalin and naringenin significantly reduced swarming motility compared to swimming motility.

Shariff *et al.* (2022) stated that combination of sub-lethal doses of Phenyllactic acid and eugenol retarded the swarming motility in *Pseudomonas aeruginosa PAO1*. Singh *et al.* (2019) also observed that the swarming motility of *Pseudomonas aeruginosa PAO1* was decreased on treatment with the extract of *Exiguobacterium indicum* SJ16 from rhizophore of *Cyperus laevigatus*. In the present study, all three

compounds decreased the motilities of *Pseudomonas aeruginosa PAO1* and thereby reduced the biofilm development. The motilities in *Pseudomonas aeruginosa* are regulated by the QS circuit. The compounds selected in the present study reduced the motilities of *Pseudomonas aeruginosa PAO1*, possibly by interfering with the QS network.

Table 17

Diameter of swarming motility zone exhibited by *Pseudomonas aeruginosa PAO1* in treated and untreated conditions

S. No	Treatment	Concentration	Diameter of swarming zone (mm)
1	Untreated Control	-	37.6 ± 0.57
2	DMSO	-	35.9 ± 1.26
3	Ciprofloxacin	½ MIC	2.8 ± 0.25**
4	C1	½ MIC	4.8 ± 0.28**
		¼ MIC	6.6 ± 0.57**
5	C2	½ MIC	5.6 ± 0.57**
		¼ MIC	6.6 ± 1.85**
6	C3	½ MIC	6.5 ± 0.50**
		¼ MIC	7.3 ± 0.57**

The data represent the mean value of three independent experiments; *p<0.05, **p<0.01

In Phase II, parameters namely prevention of biofilm development, disruption of preformed biofilm and suppression of exopolysaccharides, alginate, and total protein production were evaluated for the selected compounds. The results demonstrated that the tested compounds significantly reduced all the parameters mentioned and thereby indicating their strong antibiofilm activity against *Pseudomonas aeruginosa PAO1*. The test compounds ability to kill the metabolically active cells in biofilm further demonstrated their effectiveness as a stronger biofilm inhibitor. The antiquorum sensing capacity of the compounds was demonstrated by their potency to hinder the violacein pigment production in *Chromobacterium violaceum* and to inhibit the motility such as swimming and swarming in *Pseudomonas aeruginosa PAO1*.

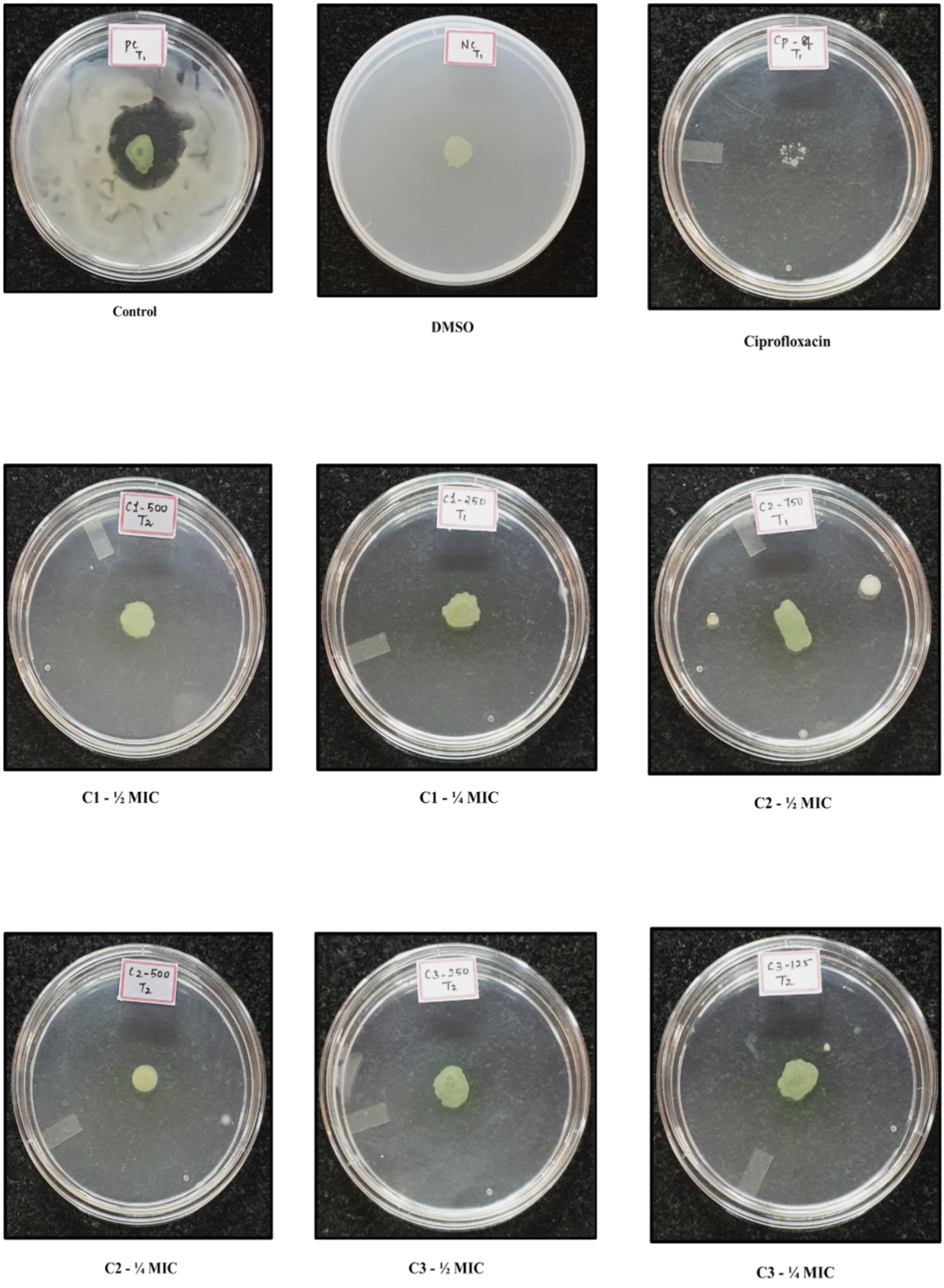

Control | DMSO | Ciprofloxacin

C1 - ½ MIC | C1 - ¼ MIC | C2 - ½ MIC

C2 - ¼ MIC | C3 - ½ MIC | C3 - ¼ MIC

Plate 6

Effect of compounds on swarming motility of *Pseudomonas aeruginosa PAO1*

Thus, from the findings of Phase II, it was revealed that the three compounds selected in the present study namely CACPD2011a-0001928786 - (3-[2-(3,4-dimethoxyphenyl)-2-(1H-indol-3-yl)ethyl]-1-(2-fluorophenyl)urea) (C1), CACPD2011a-0001927437 - (3-(4-fluorophenyl)-2-[(3-methylquinoxalin-2-yl)methylsulfanyl]quinazolin-4-one) (C2), and CACPD2011a-0000896051 - (2-({4-[4-(2-methoxyphenyl)piperazin-1-yl]pyrimidin-2-yl}sulfanyl)-N-(2,4,6 trimethylphenyl) acetamide) (C3) possessed good antibiofilm and antiquorum sensing activity against *Pseudomonas aeruginosa PAO1*.

4.3. Phase III: Evaluation of compounds on quorum sensing mediated virulence factors production in *Pseudomonas aeruginosa*

The virulence factors produced during biofilm development in *Pseudomonas aeruginosa* would provide a conducive environment to influence pathogenesis within the hosts. Regulation of biofilm formation and pathogenic invasion greatly affect secretion of virulence factors in *Pseudomonas aeruginosa* (Li *et al.*, 2017). Extracellular virulence factors secreted by *Pseudomonas aeruginosa* serve as markers to evaluate the ideal performance of the QS networks (Rather *et al.*, 2022). The efficiency of inhibitors on the secretion of quorum sensing dependent virulence factors namely pyocyanin, rhamnolipid, total protease, elastase, alkaline protease, and lipase were evaluated to confirm their antiquorum sensing ability further.

4.3.1. Pyocyanin production

Pyocyanin (N-methyl-1-hydroxyphenazine) is a bluish-green phenazine pigment that plays a predominant role during the progression and pathogenesis of infections in *Pseudomonas aeruginosa*. It is a redox secondary metabolite that mediates iron chelation and produces reactive oxygen species by concurrently reducing oxygen and oxidizing reduced glutathione in living cells.

It modifies the host's immune response to establish chronic infections by invading the host's immune system (Jabłońska *et al.*, 2022). Therefore, the evaluation of pyocyanin inhibition would assess the effectiveness of the compounds as a quorum sensing inhibitor. The pyocyanin concentration was expressed as absorbance at 520 nm, and the results are presented in Table 18.

The optical density at 520 nm was recorded as 0.58 ± 0.09 in the untreated control. In the presence of inhibitor C1 at ½ and ¼ MIC, absorbance was reduced to 0.12 ± 0.005 and 0.16 ± 0.01, respectively. The absorbance was decreased to 0.13 ± 0.02 and 0.19 ± 0.06 in the culture supernatant of *Pseudomonas aeruginosa PAO1* exposed to ½ and ¼ MIC of C2, respectively. The absorbance was found as 0.18 ± 0.05 and 0.20 ± 0.08 at ½ and ¼ MIC of C3.

Table 18 revealed that pyocyanin production in *Pseudomonas aeruginosa PAO1* was greatly affected at subinhibitory concentrations of C1, C2, and C3. On treatment with ½ MIC of C1, C2, and C3, production of pyocyanin was decreased to 79%, 78% and 69%, respectively. Treatment with ¼ MIC of C1, C2, and C3 attenuated pyocyanin production to 72%, 68%, and 65%, respectively. Among the three compounds, C1 showed the maximum (79%) inhibition of pyocyanin production at a concentration of 500 µM (½ MIC) and the minimum inhibition percentage of 65% was exhibited by C3 at its ¼ MIC (125 µM). The antibiotic ciprofloxacin showed a pyocyanin inhibition percentage of 79%, which was comparable with the selected compound C1.

The findings are on par with the results of Teerapo *et al.* (2019), who have stated that pyocyanin production in *Pseudomonas aeruginosa* was significantly ($p<0.05$) reduced to 39.84%-52.06% on treatment with BmKn-22, a scorpion venom peptide derivative. Similarly, Anju *et al.* (2022) stated that hispidulin at 75 µg/ml concentration decreased the production of pyocyanin by 81%. Tao *et al.* (2022) observed that *Potentilla kleiniana Wight* extract reduced the pyocyanin production of *Pseudomonas aeruginosa PAO1* to 84% at 800 µg/ml.

4.3.2. Rhamnolipid production

Rhamnolipids are essential components for the dispersion of biofilm, and the swarming motility of *Pseudomonas aeruginosa*. They serve as protective shields against the host's innate immune system. Inhibition of rhamnolipid is essential as it aids in creating and maintaining fluid channels around the biofilm base that help in circulating the oxygen and water flow across the cells in the biofilm (Rashiya *et al.*, 2021). Hence, the reduction in rhamnolipid production by *Pseudomonas aeruginosa PAO1* treated with compounds was analysed. The results are expressed as absorbance at 421nm (Table 19).

Table 18

Effect of compounds on pyocyanin production in *Pseudomonas aeruginosa PAO1*

S.No	Treatment	Concentration	Pyocyanin production (OD_{520})
1	Untreated Control	-	0.58 ± 0.09
2	DMSO	-	0.54 ± 0.04
3	Ciprofloxacin	½ MIC	0.12 ± 0.005** (79%)
4	C1	½ MIC	0.12 ± 0.005** (79%)
		¼ MIC	0.16 ± 0.01** (72%)
5	C2	½ MIC	0.13 ± 0.02** (78%)
		¼ MIC	0.19 ± 0.06** (67%)
6	C3	½ MIC	0.18 ± 0.05** (69%)
		¼ MIC	0.20 ± 0.08** (66%)

Values in parentheses indicate percent reduction in pyocyanin production over control

The data represent the mean value of three independent experiments; *p<0.05, **p<0.01

Table 19

Effect of compounds on rhamnolipid production in *Pseudomonas aeruginosa PAO1*

S.No	Treatment	Concentration	Rhamnolipid production (OD_{421})
1	Untreated Control	-	1.42 ± 0.24
2	DMSO	-	1.37 ± 0.06
3	Ciprofloxacin	½ MIC	0.34 ± 0.07** (76%)
4	C1	½ MIC	0.37 ± 0.03** (74%)
		¼ MIC	0.44 ± 0.03** (69%)
5	C2	½ MIC	0.44 ± 0.09** (69%)
		¼ MIC	0.50 ± 0.05** (65%)
6	C3	½ MIC	0.41 ± 0.08** (71%)
		¼ MIC	0.47 ± 0.07** (67%)

Values in parentheses indicate percent reduction in rhamnolipid production over control

The data represent the mean value of three independent experiments; *p<0.05, **p<0.01

It was evident that the production of rhamnolipids was significantly ($p<0.01$) affected by treatment with all three compounds. At the ½ MIC level, the absorbance was reduced from 1.42 ± 0.24 (untreated control) to 0.37 ± 0.03, 0.44 ± 0.09, and 0.41 ± 0.08 for C1, C2, and C3, respectively. It also shows a notable reduction in absorbance for all three selected compounds at their ¼ MIC dose.

The percent reduction in rhamnolipid production by C1, C2, and C3 at their ½ MIC level were up to 74%, 69%, and 71%, respectively. However, the inhibition percentage of rhamnolipid production at ¼ MIC dosage of C1, C2, and C3 was 69%, 64%, and 67%, respectively. C1 imparted the highest inhibition (74%) of rhamnolipid production at its ½ MIC dose of 500 µM. The percent reduction of rhamnolipid production of selected compound C1 is on par with ciprofloxacin.

These results were in line with the report of Karuppiah *et al.* (2021), who found that production of rhamnolipid decreased in *Pseudomonas aeruginosa PAO1* by 68% on treatment with 1,8-cineole at a 100 µg/ml concentration. Singh *et al.* (2017) stated that 0.1 mg/ml of bacterial extract of *Delftia tsuruhatensis* reduced rhamnolipid production to 85% and 67% in *Pseudomonas aeruginosa PAO1* and *Pseudomonas aeruginosa PAH* strains respectively. Parasuraman *et al.* (2020) affirmed that fungal extract of *Pestalotiopsis sydowiana* at 250 µg/ml and 500 µg/ml concentrations inhibited rhamnolipid production by *Pseudomonas aeruginosa PAO1* to 43.14% and 61.09%, respectively.

4.3.3. Total protease activity

Proteases are crucial in forming biofilm, motility, and generation of antibiotic resistance in *Pseudomonas aeruginosa*. These are hydrolytic enzymes that counteract the effects of the host defense system and aid in the damage of host tissues. *Pseudomonas aeruginosa* produces different types of extracellular proteases, namely protease IV, alkaline protease, elastase A (*lasA*), and elastase B (*lasB*) (Ganesh and Rai, 2017; Andrejko *et al.*, 2013; Kida *et al.*, 2013; Drenkard, 2003).

The protease helps *Pseudomonas aeruginosa* to colonize the host tissues more effectively and contributes significantly to formation of biofilm (Qadri *et al.*, 2016). Thus, the effect of compounds on the total protease secretion in *Pseudomonas aeruginosa PAO1* was evaluated using skim milk agar plates. The total protease activity was assessed by measuring the zone of clearance (mm), and the results are given in Table 20 and Plate 7.

The results revealed a decrease in protease activity with a zone of clearance (mm) of 5.1 ± 0.28 mm, 6.1 ± 0.28 mm, and 6.0 ± 0 mm on treatment with ½ MIC of C1, C2, and C3, respectively compared to the untreated control (14.6 ± 0.57 mm). A similar pattern was seen on treatment with ¼ MIC dosage of compounds, with a zone clearance of 7.0 ± 0 mm, 7.3 ± 0.57 mm, and 7.0 ± 0 mm for C1, C2, and C3, respectively. The highest inhibitory effect on the total protease activity was shown by C1 at a concentration of 500 µM (½ MIC). The antibiotic ciprofloxacin exhibited no clearance zone in the skim milk agar plate.

Table 20
Effect of compounds on total protease activity in *Pseudomonas aeruginosa PAO1*

S.No	Treatment	Concentration	Zone of clearance (mm)
1	Untreated Control	-	14.6 ± 0.57
2	DMSO	-	12.33 ± 0.47
3	Ciprofloxacin	½ MIC	Nil
4	C1	½ MIC	5.1 ± 0.28**
		¼ MIC	7.0 ± 0**
5	C2	½ MIC	6.1 ± 0.28**
		¼ MIC	7.3 ± 0.57**
6	C3	½ MIC	6.0 ± 0**
		¼ MIC	7.0 ± 0**

The data represent the mean value of three independent experiments; *p<0.05, **p<0.01

These results were on par with Khan *et al.* (2019), who reported a reduced protease activity in skim milk agar plates containing *Pseudomonas aeruginosa* treated with chitosan-polypyrrole nanocomposites. Chatterjee *et al.* (2021) reported a decrease in the total proteolytic activity of *Pseudomonas aeruginosa PAO1* on treatment with cuminaldehyde. Kiran *et al.* (2021) also documented that lipoprotein at 50 µg/ml inhibited protease activity in *Pseudomonas aeruginosa* with zone of clearance 12 mm compared to the untreated control (32 mm).

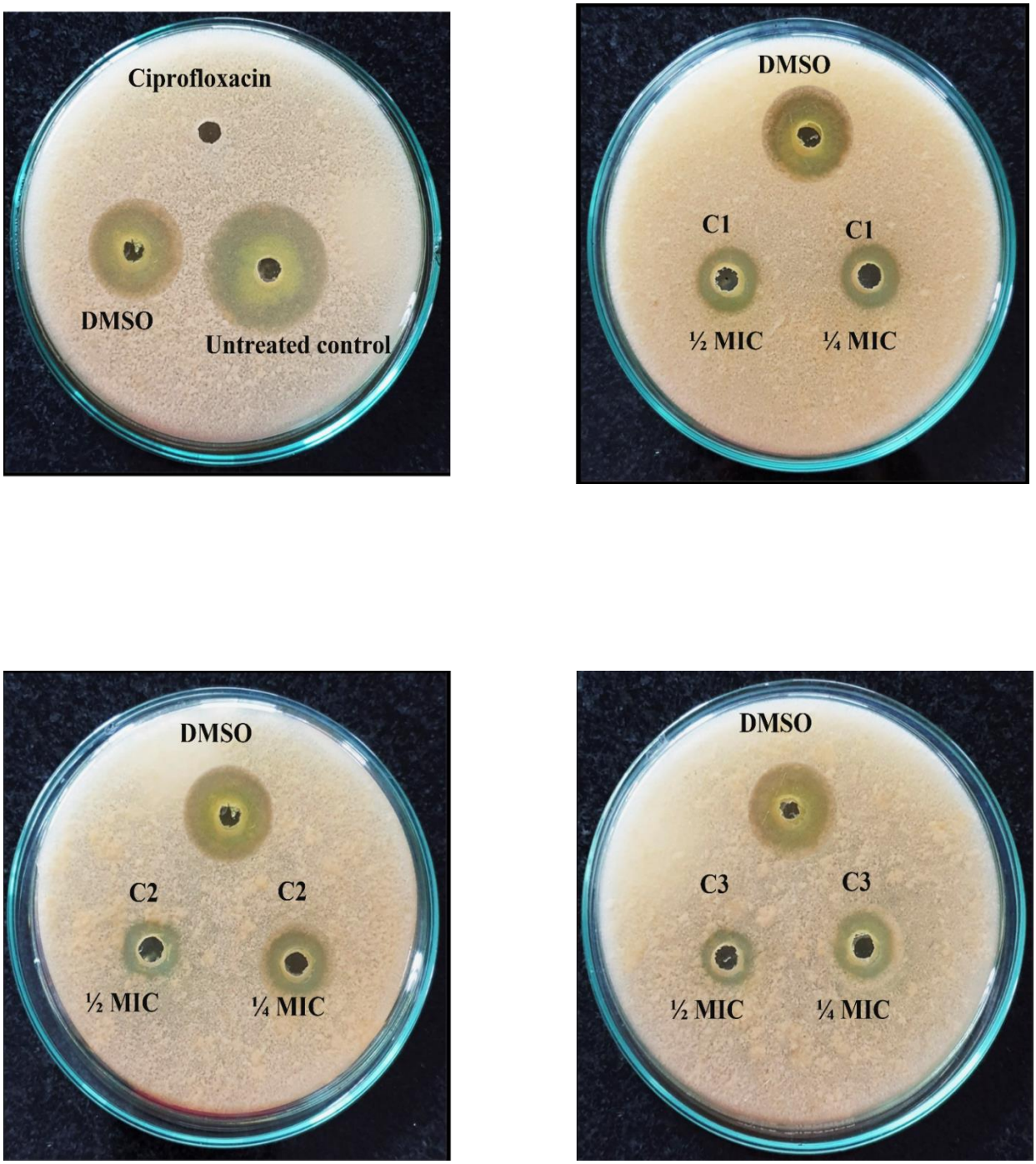

Plate 7

Zone of protease clearance exhibited by *Pseudomonas aeruginosa PAO1* in treated and untreated conditions

4.3.3.1. *LasB* elastase activity

LasB elastase contributes to the pathogenesis of *Pseudomonas aeruginosa* infection in the respiratory tract. *LasB* elastase aids bacteria in colonizing and destroying host tissues. Elastases damage the host tissues by hydrolysing the extracellular matrix components and tight junctions in the plasma membrane, which helps *Pseudomonas aeruginosa* to pass through the host's endothelial and epithelial barriers (Das *et al.*, 2016; Kuang *et al.*, 2011; Antunes *et al.*, 2010). Therefore, to study the effectiveness of compounds on elastase B activity, the expression profile of the *lasB* gene of *Pseudomonas aeruginosa PAO1* in untreated and treated conditions was quantified by qRT-PCR, and the results are presented in Figure 37.

It was observed that C1 drastically suppressed the expression of *the lasB* gene (87%). The compound C2 significantly ($p<0.01$) downregulated the gene expression of *lasB* (53%). The other compound C3 was also able to downregulate the expression of *lasB* (29%) but not as effective as the other two compounds. Thus, these findings demonstrated that the three compounds have the ability to lower the activity of elastase in *Pseudomonas aeruginosa PAO1*.

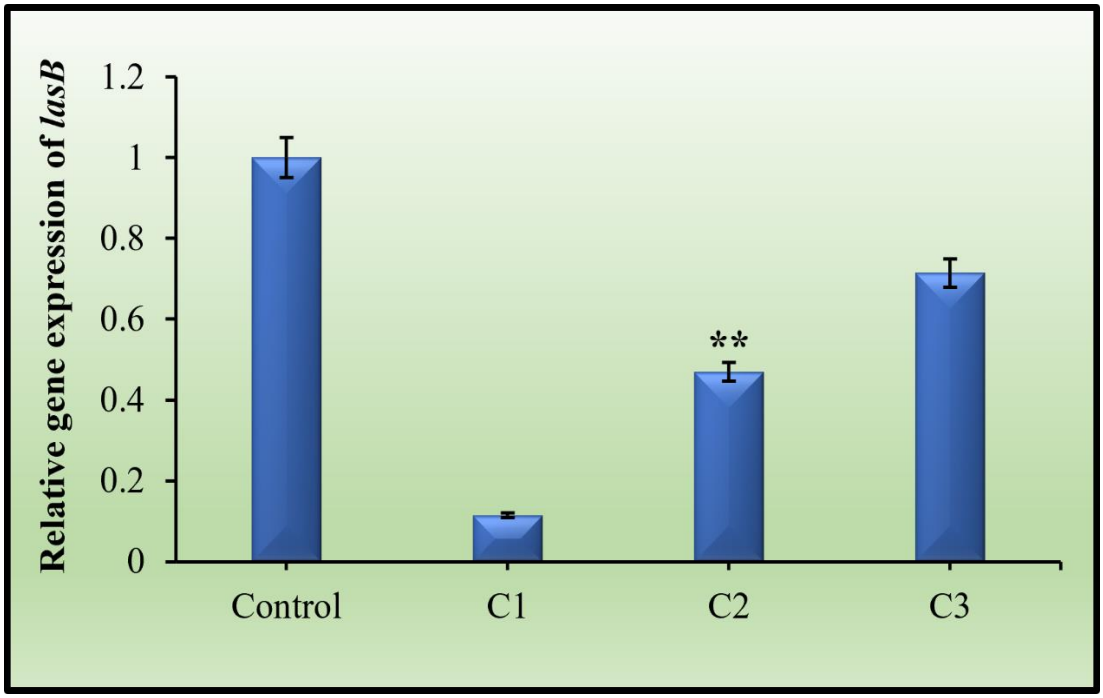

Figure 37

Relative gene expression of *lasB* quantified by qRT-PCR

In connection with this finding, Namasivayam *et al.* (2022) described that chitosan-selenium bio nanocomposite (50-100 μg/ml) significantly ($p<0.05$) reduced the expression level of *LasB* gene in *Pseudomonas aeruginosa*. Zhao *et al.* (2022) suggested that *LasB* elastolytic activity was significantly declined ($p<0.01$, $p<0.001$) on treating *Pseudomonas aeruginosa PAO3* strain to azithromycin and a natural isoquinoline alkaloid berberine.

Tao *et al.* (2022) noticed that *Potentilla kleiniana Wight* extract decreased the elastase activity of *lasB* in *Pseudomonas aeruginosa.* Bajire *et al.* (2021) evidenced that 6-methyl coumarin at a concentration of 120 μg/ml and 250 μg/ml exhibited a more than 80% decrease in the elastase activity of *Pseudomonas aeruginosa PAO1*. Luo *et al.* (2017) reported that sub-MICs of baicalin extracted from *Scutellaria baicalensis* suppressed the *LasB* elastase activity to 77.1-93.6%.

4.3.3.2. Alkaline protease activity

Alkaline protease (*AprA*) is a metalloprotease that is actively involved in the hydrolyzation of proteins such as matrix metalloproteinases, complement factors, cytokines, human IFN-γ and TNF-α (Aybey and Demirkan, 2016). *AprA* supresses host immune system and inhibit complement mediated phagocytosis (Lee *et al.,* 2018; Laarman *et al.,* 2012). The selected compounds were evaluated for their effect on the alkaline protease activity of *Pseudomonas aeruginosa PAO1* by measuring the absorbance at 590 nm. The results of the alkaline protease activity are provided in Table 21.

The absorbance at 590nm was 0.80 ± 0.08 in untreated *Pseudomonas aeruginosa PAO1* cells. Treatment with compounds C1, C2, and C3 at ½ and ¼ MIC dosage reduced the optical density value at 590 nm compared with untreated control. The results inferred that the alkaline protease activity of *Pseudomonas aeruginosa PAO1* was significantly ($p<0.01$) inhibited up to 70%, 69%, and 68% in the presence of ½ MIC of C1, C2, and C3, respectively.

At ¼ MIC dose, inhibition in alkaline protease production was found to be 62%, 54%, and 51% for C1, C2, and C3, respectively. The maximum inhibitory effect on alkaline protease production was exhibited by C1 (70%) followed by C2 (69%) at its ½ MICs of 500 μM and 250 μM, respectively. The positive control, ciprofloxacin revealed an inhibition percentage of 72% on the production of alkaline protease in *Pseudomonas aeruginosa PAO1*.

Aybey and Demirkan, (2016) reported a good inhibitory effect on alkaline protease production by *Pseudomonas aeruginosa PAO1* on treatment with human serum paraoxonase 1 (hPON1) at 0.1 mg/ml. Bose *et al.* (2020) stated that expression of *AprA* gene was downregulated on treatment with nano encapsulated α-terpineol.

Similarly, Di Bonaventura *et al.* (2022) also observed that the "non-antibiotic" drugs ciclopirox, ribavirin, 5-fluorouracil, and tobramycin reduced the *AprA* gene expression in *Pseudomonas aeruginosa PAO1*. Abd El-Aziz *et al.* (2017) affirmed that clove buds and cumin seeds extracts at its sub-MICs reduced alkaline protease production in *Pseudomonas aeruginosa* by showing a clear zone in skimmed milk agar plates.

Table 21
Effect of compounds on alkaline protease activity in *Pseudomonas aeruginosa PAO1*

S.No	Treatment	Concentration	Alkaline protease activity (OD_{590})
1	Untreated Control	-	0.80 ± 0.08
2	DMSO	-	0.75 ± 0.07
3	Ciprofloxacin	½ MIC	$0.22 \pm 0.03^{**}$ (73%)
4	C1	½ MIC	$0.24 \pm 0.08^{*}$ (70%)
		¼ MIC	$0.30 \pm 0.03^{**}$ (63%)
5	C2	½ MIC	$0.25 \pm 0.03^{**}$ (69%)
		¼ MIC	$0.37 \pm 0.12^{**}$ (54%)
6	C3	½ MIC	$0.25 \pm 0.01^{**}$ (69%)
		¼ MIC	$0.38 \pm 0.16^{**}$ (53%)

Values in parentheses indicate percent reduction in alkaline protease activity over control
The data represent the mean value of three independent experiments; $^{*}p<0.05$, $^{**}p<0.01$

4.3.4. Lipase activity

The coordination of motility along gradients is primarily regulated by lipolytic enzymes produced by *Pseudomonas aeruginosa* (Rosenau *et al.,* 2010). Lipolytic enzymes, specifically lipase of *Pseudomonas aeruginosa*, namely LipA and LipC hold a significant role in the coordinated behavior of type IV pili and flagella-driven motility (Miller *et al.,* 2008). Therefore, the selected compounds were investigated for their ability to inhibit lipase production in *Pseudomonas aeruginosa PAO1* by measuring the absorbance at 400nm. The results of the lipase activity are given in Table 22.

The absorbance was decreased to 0.62 ± 0.09, 0.62 ± 0.02, and 0.79 ± 0.03 for the compounds C1, C2, and C3 at ½ MIC dose, respectively, on comparison with untreated control (2.88 ± 0.09). On the other hand, in *Pseudomonas aeruginosa PAO1* exposed to ¼ MIC of C1, C2, and C3, the absorbance was 0.67 ± 0.06, 0.70 ± 0.02, and 0.83 ± 0.08 respectively.

The lipase activity was inhibited to 78%, 77%, and 73% when treated with ½ MIC dose of C1, C2, and C3, respectively. The lipase activity was retarded up to 77%, 76%, and 71% upon treatment with ¼ MIC of C1, C2, and C3, respectively. Among the three compounds, the highest inhibitory effect on lipase production was shown by C1 (78%) at a concentration of 500 μM (½ MIC). Ciprofloxacin inhibited lipase production in *Pseudomonas aeruginosa PAO1* with an inhibition percentage of 78% comparable to compound C1.

Abdel-Rhman *et al.* (2020) observed that sub-MICs of QSIs, namely tyrosol (natural compound) and EDTA (polyamine carboxylic acid), significantly ($p<0.001$) reduced the production of lipase in *Pseudomonas aeruginosa* by ≥63%. Gbian and Omri, (2021) reported that the liposome-encapsulated erythromycin and gentamicin in combination with phenylalanine arginine beta-napthylamide (PABN) decreased the lipase activity of *Pseudomonas aeruginosa PAO1.* Kiran *et al.* (2021) inferred that lipopeptide at a 50 μg/ml concentration inhibited lipase production in *Pseudomonas aeruginosa FSPA02* without affecting the bacterial growth.

Table 22
Effect of compounds on lipase activity in *Pseudomonas aeruginosa PAO1*

S.No	Treatment	Concentration	Lipase activity (OD_{400})
1	Untreated Control	-	2.88 ± 0.09
2	DMSO	-	2.82 ± 0.41
3	Ciprofloxacin	½ MIC	0.63 ± 0.01** (78%)
4	C1	½ MIC	0.62 ± 0.09* (78%)
		¼ MIC	0.67 ± 0.06** (77%)
5	C2	½ MIC	0.66 ± 0.02** (77%)
		¼ MIC	0.70 ± 0.02** (76%)
6	C3	½ MIC	0.79 ± 0.03** (73%)
		¼ MIC	0.83 ± 0.08** (71%)

Values in parentheses indicate percent reduction in lipase activity over control
The data represent the mean value of three independent experiments; *p<0.05, **p<0.01

In Phase III, the impact of compounds on quorum sensing mediated virulence factor production was studied. The results inferred that all three compounds were able to hinder the production of pyocyanin, rhamnolipid, protease, and lipase activity above 50% which are comparable with positive control ciprofloxacin. The gene expression analysis of *lasB* activity further affirmed the antiquorum sensing ability of the tested compounds. The findings of phase III revealed that the ½ MIC dose of compounds were found to be more effective than ¼ MIC against *Pseudomonas aeruginosa PAO1*. Hence, further studies were carried out at ½ MIC of C1 (43.3 µg/ml), C2 (42.8 µg/ml), and C3 (23.8 µg/ml), respectively.

4.3.5. Morphology analysis

4.3.5.1. Field emission scanning electron microscopy

A high-definition field emission scanning electron microscope (FESEM) was used to observe the structural modulation of the *Pseudomonas aeruginosa PAO1* biofilms. The morphological and structural changes of the *Pseudomonas aeruginosa PAO1* biofilm in untreated and treated with ½ MIC of compounds were observed using field emission scanning electron microscopy, and the results are shown in Figure 38.

The observations revealed that the control group (Figure 38a) appeared as a dense multi-layered EPS matrix with many colonies of varying sizes. In contrast, the treated groups showed a reduction in biofilm biomass and were found to be scattered in appearance. The FESEM analysis confronts the efficacy of the selected compounds as potent disruptors of *Pseudomonas aeruginosa PAO1* biofilms. In addition, the FESEM analysis confirmed that the compounds at their sub-MICs completely lacked bactericidal effects.

The samples treated with C1 showed a drastic reduction in cell attachment to the surface (Figure 38b), whereas C2 exhibited an enhanced dispersal effect on *Pseudomonas aeruginosa PAO1* biofilms (Figure 38c). The architecture of biofilm on treatment with C3 was observed as elongated fibril with limited clumping and colonization (Figure 38d). Thus, FESEM results further confirmed our *in vitro* studies and proved that the compounds could reduce biofilm by preventing and disrupting bacterial cell attachment to the surface. These results agreed with the report by Qais *et al.* (2021), who demonstrated the same pattern of biofilm inhibition on treatment with gold nanoparticle synthesized using *Capsicum annum* extract.

Khan *et al.* (2019) also suggested that sub-MICs of chitosan-polypyrrole nanocomposites exhibited complete inhibition of *Pseudomonas aeruginosa PAO1* cell attachment to the surface. Luo *et al.* (2017) stated that SEM analysis of 24 hrs and 96 hrs *Pseudomonas aeruginosa* biofilms treated with a plant-derived flavone baicalin showed a decreased extracellular matrix.

Dahibhate *et al.* (2022) described that SEM analysis of *Pseudomonas aeruginosa PAO1* biofilms portrayed a well-established biofilm with adhered cells in the control group. In contrast, the cells were found to be dispersed upon treatment with ethyl acetate extract of *Bruguiera gymnorhiza*.

The results of FESEM analysis inferred that C1, C2, and C3 were able to alter biofilm architecture and cell morphology of *Pseudomonas aeruginosa PAO1*. It was seen that ½ MIC of the selected LasR inhibitors substantially inhibited cell attachment to the surface thereby suggesting the compounds as an effective biofilm disruptor.

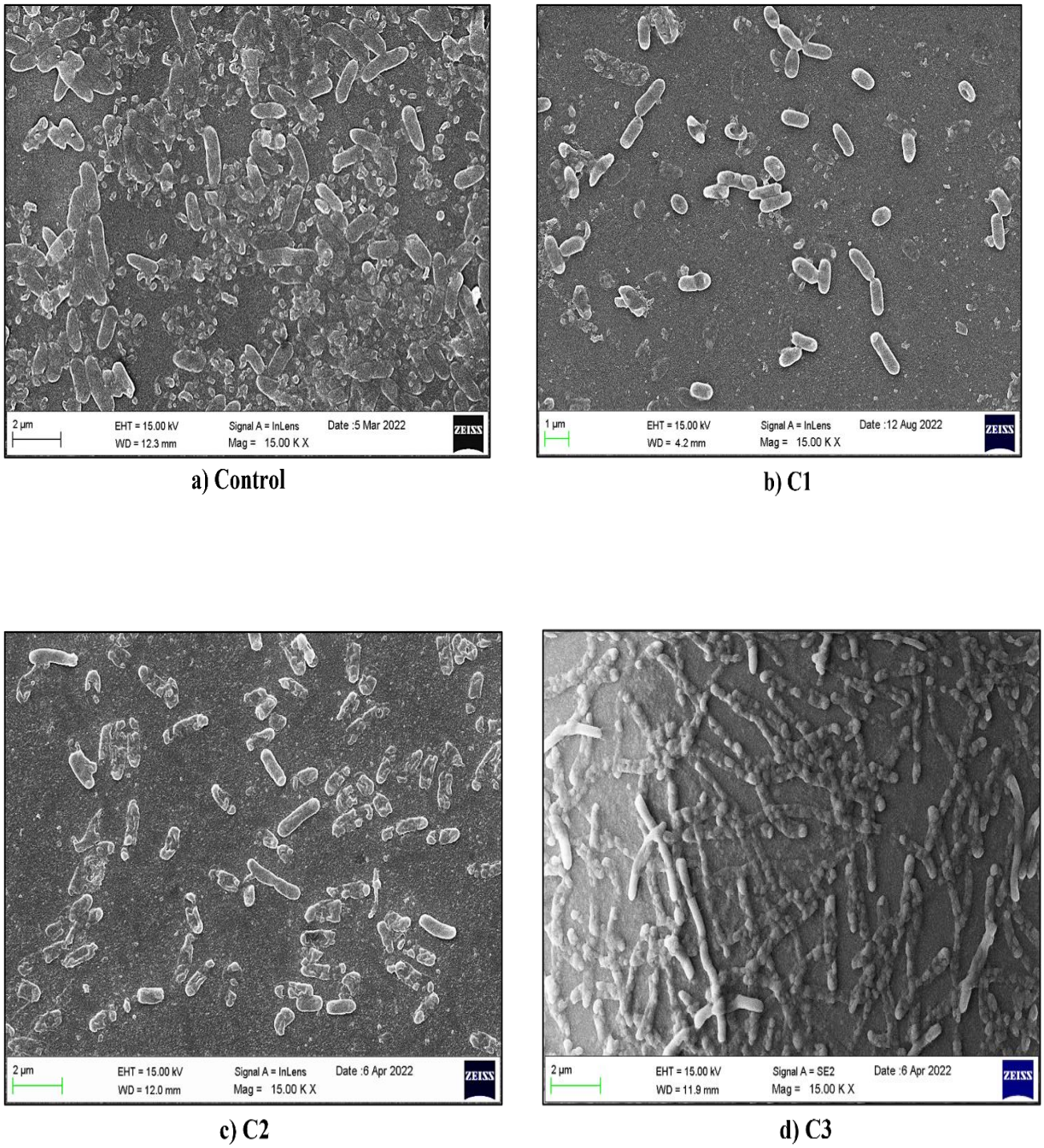

Figure 38
FESEM analysis of *Pseudomonas aeruginosa PAO1* biofilm architecture

Thus, the results of Phase III demonstrated that the three selected compounds namely CACPD2011a-0001928786 - (3-[2-(3,4-dimethoxyphenyl)-2-(1H-indol-3-yl)ethyl]-1-(2-fluorophenyl)urea) (C1), CACPD2011a-0001927437 - (3-(4-fluorophenyl)-2-[(3-methylquinoxalin-2-yl)methylsulfanyl]quinazolin-4-one) (C2), and CACPD2011a-0000896051 - (2-({4-[4-(2-methoxyphenyl)piperazin-1-yl]pyrimidin-2-yl}sulfanyl)-N-(2,4,6 trimethylphenyl) acetamide) (C3) could serve as an effective leads for developing antibiofilm and antiquorum sensing agent against LasR in *Pseudomonas aeruginosa.*

4.4. Phase IV: Investigation of the influence of selected compounds on the expression profile of quorum sensing regulatory genes

4.4.1. Quantification of relative gene expression of quorum sensing regulatory genes

The transcriptional regulator *las/rhl* system is particularly prominent among the intricate hierarchical network of genes involved in *Pseudomonas aeruginosa* QS because it directly regulates several genes linked to QS-regulated virulence factors production (Parai *et al.,* 2018; Sharma *et al.,* 2014; Balasubramanian *et al.,* 2013).

The autoinducer molecules of *las* and *rhl* systems, namely N-3-oxododecanoyl-L-homoserine lactone (3-oxo-C12-HSL) and N-butanoyl-L-homoserine lactone (C4-HSL) synthesized by *lasI* and *rhlI* genes serve as transcriptional activators to mediate the secretion of the virulence factors that drive biofilm-associated pathogenesis in *Pseudomonas aeruginosa*. Apart from these two QS systems, the third QS system *pqs* are also linked to formation of biofilm and virulence factors in *Pseudomonas aeruginosa.* The three systems are interlinked in a hierarchical pattern, with the *las* system controlling the *rhl* and *pqs* systems (Smith, 2003).

The effect of compounds on the expression of QS-regulatory genes, namely *lasI, lasR, rhlI, rhlR, pqsA* and *pqsR* were studied at their ½ MIC dosage by quantitative real-time PCR (qRT-PCR). The housekeeping gene glyceraldehyde-3-phosphate dehydrogenase (GAPDH) was used to normalize gene expression. The relative expression level of quorum sensing genes was calculated using $2^{-\Delta\Delta CT}$ method and is depicted in Figure 39.

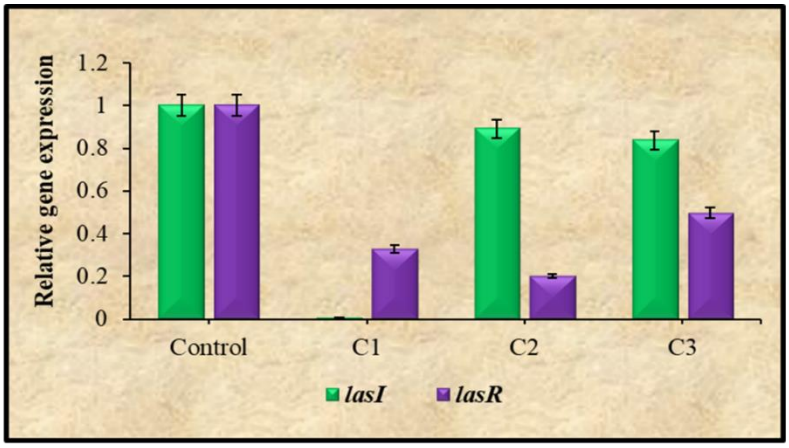

The data represent the mean value of three independent experiments; *p< 0.05, **p <0.01 vs control

a) *Las* system

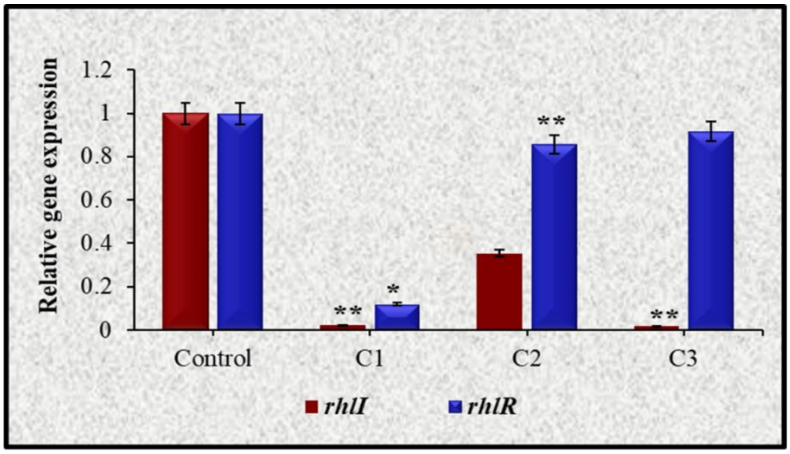

The data represent the mean value of three independent experiments; *p< 0.05, **p <0.01 vs control

b) *Rhl* system

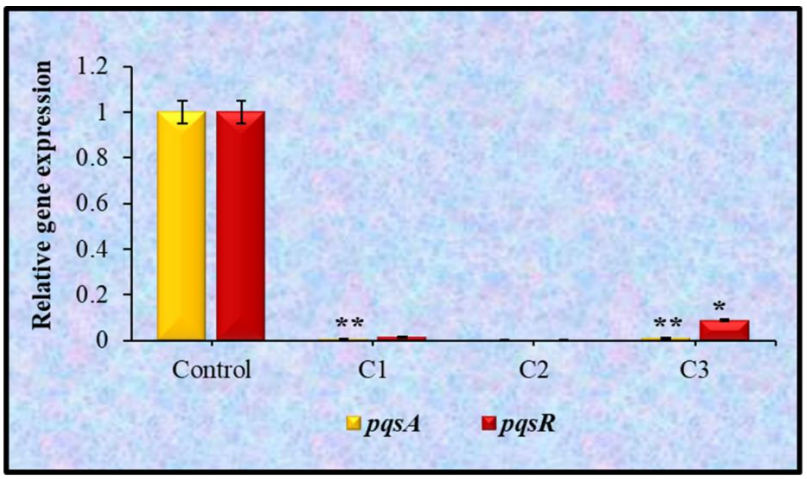

The data represent the mean value of three independent experiments; *p< 0.05, **p <0.01 vs control

c) *Pqs* system

Figure 39

Relative gene expression analysis of QS-regulatory genes of *Pseudomonas aeruginosa PAO1* by qRT-PCR

Figure 39a revealed that treatment with ½ MIC of C1 significantly ($p<0.01$) suppressed *lasI* and *lasR* expression by 99.34% and 67.17%, respectively. C2 and C3 downregulated the *lasR* gene expression by 79.75% and 50.35%, respectively. In the case of *lasI* gene, C2 and C3 suppressed the between 11% to 16% compared to untreated control. The *rhlI* and *rhlR* expression (Figure 39b) was drastically decreased by 97.95% and 88.15% for C1 compared to the untreated control. C2 and C3 significantly ($p<0.01$) reduced the expression of *rhlI* by 64.57% and 98.13%, respectively, whereas the expression of *rhlR* was decreased by 14.35% and 8.41% in comparison with control.

In the case of *pqs* system, all three compounds were able to downregulate the expression of *pqsA* and *pqsR* by more than 90% (Figure 39c). The relative gene expression analysis of QS-regulatory genes of *Pseudomonas aeruginosa PAO1* revealed that compound C1 significantly downregulated the expression of all three QS systems by more than 90% compared to untreated *Pseudomonas aeruginosa PAO1*. The compounds C2 and C3 did not drastically reduce the expression level of *lasI/R* and *rhlI/R* genes, but they significantly decreased the expression level of these genes.

The results of qRT-PCR agreed with Zhong *et al.* (2020), who observed that catechin 7-xyloside, sappanol and butein downregulated the QS-regulated genes namely *lasI, lasR, rhlI,* and *rhlR* genes. Parasuraman *et al.* (2020) evidenced that the QS regulatory genes of *Pseudomonas aeruginosa PAO1* were found to be reduced significantly on treatment with marine fungal extract of *Pestalotiopsis sydowiana.* Similarly, previous studies have shown that *Dioon spinulosum* extract (Elekhnawy *et al.,* 2022), tyrosol (Abdel-Rhman *et al.,* 2020), and BmKn-22 scorpion venom peptide (Teerapo *et al.,* 2019) significantly downregulated QS regulatory genes. The gene expression analysis of quorum sensing regulatory genes further validated that the selected compounds inhibited secretion of virulence factors and biofilm development in *Pseudomonas aeruginosa PAO1* by downregulating the transcription of QS regulatory genes.

4.4.2. Evaluation of antagonistic efficacy of LasR inhibitors by β-galactosidase reporter gene

Transcriptional fusions have been shown to be crucial tools for understanding how genes are expressed and regulated in living systems. Using reporter genes substantially simplifies the task of observing promoter activity (Flores-Sandoval *et al.,* 2015). Herein we have used the plasmid pKDT17 transformed with a translational fusion of *lasB::lacZ* gene

coupled to LasR. The plasmid serves as a reporter to quantify the effectiveness of selected inhibitors on LasR expression. Loss of LasR binding to downstream gene promoters will hinder the expression of QS-regulated genes and further affect the virulence traits of *Pseudomonas aeruginosa.* Thus, the reporter gene (*lasB::lacZ*) assay quantifies LasR activity, which is indicated by its binding to the *lasB* promoter and activation of β-galactosidase fusion protein, with the resulting enzyme activity being detected in a Miller assay.

The purpose of antagonists is to bind to LasR and stabilize it to a confirmation that prevents it from binding to DNA. When LasR links to its autoinducer and binds to DNA, it interacts with RNA polymerase and mediates the regulation of gene expression. Hence, many antagonists are effectively designed to disrupt this interaction between LasR and its ligand (Suneby *et al.,* 2017; Amara *et al.,* 2016; O'Brien *et al.,* 2015). In this context, cell-based reporter gene assays can be employed to determine the efficiency of such antagonists (Moore *et al.,* 2015). Therefore, *in vitro* β-galactosidase reporter gene assay was done to evaluate the antagonistic efficacy of the selected inhibitors at the transcriptional level.

The selected compounds were examined for their antagonistic efficacy in the reporter gene assay at nM concentrations. The study employed 50 nM AHL as the positive control. The compounds (25-200 nM) were assessed for their antagonistic potential along with AHL, an inducer of LasR that triggers the transcriptional modifications associated with QS. These concentrations were taken since the assay was carried out based on the MIC of *Escherichia coli DH5α* cells carrying plasmid pKDT17. The LasR expression was quantified as the β-galactosidase enzyme activity and is illustrated in Figure 40.

Figure 40 shows a significant ($p<0.01$) decline in the activity of β-galactosidase at 100 nM. The activity of β-galactosidase enzyme (expressed in Miller units) in the presence of C1, C2, and C3 at 100 nM concentration were identified to be 54.46 ± 11.07, 29.18 ± 2.25, and 74.21 ± 0.23, respectively. The percentage of inhibition of β-galactosidase activity at 100 nM of C1, C2, and C3 was found to be 85%, 92%, and 79%, respectively. In line with the report of Kafle *et al.* (2016), C1, C2, and C3 also decreased the β-galactosidase activity in the presence of AHL. Khan *et al.* (2020) reported 62% decline in the activity of β-galactosidase enzyme in *Escherichia coli* harbouring reporter plasmid pKDT17 when treated with zinc oxide nanospikes (200 μg/ml). Bottomley *et al.* (2007) suggested that LasR antagonists may directly interact with the native autoinducer to generate unstable or insoluble

LasR complex by interfering with the folding of a protein. Thus, the reporter gene assay revealed that the compounds had affected the LasR's DNA binding affinity by binding to the natural ligand binding pocket in LasR.

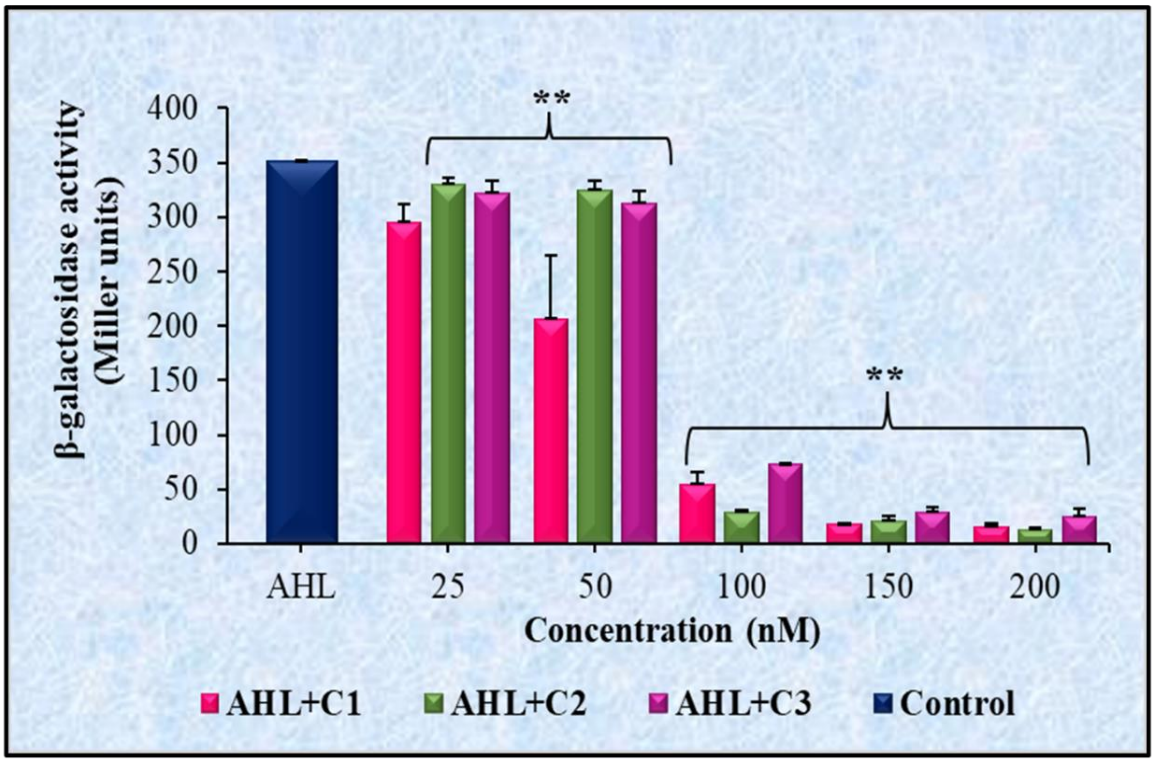

The data represent the mean value of three independent experiments; *p< 0.05, **p <0.01 vs control

Figure 40
Inhibitory effect of compounds on β-galactosidase enzyme production assayed using the *in vitro* LasR reporter gene assay

In general, *Pseudomonas aeruginosa* has hierarchical interactions within its QS system. Among them, the *las* system occupies the highest position and controls the *rhl*, *pqs*, and *iqs* systems. The *rhl* system, which is regulated by other QS systems, activates numerous QS-controlled virulence factors, and is at the lowest level. *Las* and *iqs* stimulate *pqs*, which in turn activates the *rhl* system. Finally, *las* also activates *iqs*, which controls the *pqs* and *rhl* systems. The key regulatory QS systems of *Pseudomonas aeruginosa* namely *las* and *rhl* plays a crucial role in controlling the synthesis of the virulence components and its activity. When cell density reaches a threshold, increased number of AHLs binds to the principal protein of the QS system namely *lasR* and influence the expression of key regulatory genes of QS in *Pseudomonas aeruginosa PAO1*.

The *lasIR* circuit controls the genes of *toxA* (exotoxin A), *lasA* (protease), *lasB* (elastase) and *rhlIR* system regulates genes of *rhlAB* (rhamnolipids), *lecA* (lectins), *aprA* (alkaline protease), whereas *PQS* controls *phzABCDEFG*, *phzM* (pyocyanin). Thus, it was observed that the qRT-PCR result was well corroborated with that of the inhibition in virulence factors production by the selected compounds in *Pseudomonas aeruginosa PAO1*. A significant decrease in *lasI, lasR, rhlI* and *rhlR* expression suggested that the chosen compounds inhibited virulence factors production and development of biofilm in *Pseudomonas aeruginosa* through the key regulators of QS circuitry.

Binding of QSIs to *lasR* downregulates the expression of genes necessary for elastase (*lasB*) and protease (*lasA*) activity, along with decrease in the *rhl* gene expression system. The downregulation of *rhl* system would eventually suppress the production of pyocyanin and rhamnolipid. Downregulated gene pattern of *rhlR* and *pqsR* inhibits the synthesis of pyocyanin, rhamnolipid, and swarming motility. Thus, from the findings of Phase IV, it can be affirmed that the downregulated gene expression pattern of the major quorum sensing regulatory genes namely *lasI, lasR, rhlI, rhlR, pqsA,* and *pqsR* might have led to the inhibitory effect of selected compounds on the production of the virulence factors namely pyocyanin, rhamnolipid, total protease, elastase, alkaline protease, and lipase, prevented biofilm formation and also inhibited motility behaviours in *Pseudomonas aeruginosa PAO1*. Particularly, since the compounds target LasR, it might have possibly led to the shut down of entire QS network of *Pseudomonas aeruginosa.* In addition, its impact on reducing the expression of LasR at transcriptional level confirmed the three selected compounds as a good antagonist against LasR.

Overall, the results of the present research work unveiled that the three selected inhibitors namely CACPD2011a-0001928786 - (3-[2-(3,4-dimethoxyphenyl)-2-(1H-indol-3-yl)ethyl]-1-(2-fluorophenyl)urea) (C1), CACPD2011a-0001927437 - (3-(4-fluorophenyl)-2-[(3-methylquinoxalin-2-yl)methylsulfanyl]quinazolin-4-one) (C2), and CACPD2011a-0000896051 - (2-({4-[4-(2-methoxyphenyl)piperazin-1-yl]pyrimidin-2-yl}sulfanyl)-N-(2,4,6 trimethylphenyl) acetamide) (C3) could serve as possible lead compounds for designing a potent antagonist against LasR in *Pseudomonas aeruginosa.* Hence, these compounds may further be exploited to generate a therapeutic agent with enhanced activity for managing infections associated with *Pseudomonas aeruginosa* biofilms.